International Journal of Nanomedicine

Dovepress
Taylor & Francis Group

Open Access Full Text Article

ORIGINAL RESEARCH

Anti-Infection Efficacy, Osteogenesis Potential, and Biocompatibility of 3D Printed PLGA/Nano-Hydroxyapatite Porous Scaffolds Grafted with Vancomycin/DOPA/rhBMP-2 in Infected Rabbit Bone Defects

A li mu Ke re mu[1], Maimaitiaili Abulikemu[2], Zhilin Liang[2], Abudurusuli Abulikemu[2], Aikebaier Tuxun[2]

[1]Department of Orthopedic, First People's Hospital of Kashgar, Kashgar, Xinjiang, 844000, People's Republic of China; [2]Department of Trauma Orthopaedics, First People's Hospital of Kashgar, Kashgar, Xinjiang, 844000, People's Republic of China

Correspondence: Aikebaier Tuxun, First People's Hospital of Kashgar, 120 Yingbin Avenue, Kashgar City, Kashgar Region, Xinjiang Province, People's Republic of China, Email Aikebaiert@hotmail.com

Background: Given the limitations of traditional therapies, the treatment of infected bone defects (IBD) remains a great challenge. It is urgent to find a novel method that can simultaneously eradicate infection and promote new bone formation. With the increasing application of personalized scaffolds in orthopedics, novel biomaterials with both antibacterial and osteoinductive properties have provided a viable option for IBD treatment. Through the three-dimensional (3D) printing technology, we fabricated a poly(lactic-co-glycolic acid)(PLGA)/nano-hydroxyapatite (n-HA) composite scaffold grafted with the antibiotic vancomycin and loaded with the osteoinductive agent recombinant human bone morphogenic protein-2 (rhBMP-2) via polydopamine (DOPA) chemistry, whose therapeutic effects on IBD were determined.

Methods: After examining the hydrophilicity, surface chemical composition, mechanical properties, and drug release of the PLGA/n-HA, PLGA/n-HA/VAN, and PLGA/n-HA/VAN+DOPA/rhBMP-2 composite scaffolds, pre-osteoblast MC3T3-E1 cells were seeded onto the scaffold surface to assess the biocompatibility and osteoconductive properties of the scaffolds in vitro. For in vivo experiments, the composite scaffolds contaminated with *Staphylococcus aureus* were implanted into the defect sites of rabbit radius. After 12 weeks, micro-CT analysis, H&E and Masson staining, immunohistochemistry, and viable bacteria counting were conducted to compare the effects of three composite scaffolds on new bone formation and bone infection.

Results: The surface modification with DOPA/rhBMP-2 increased the hydrophilicity of PLGA/n-HA scaffolds. Vancomycin and BMP-2 were continuously and regularly eluted from the PLGA/n-HA/VAN+DOPA/rhBMP-2 scaffolds. The PLGA/n-HA/VAN +DOPA/rhBMP-2 scaffolds promoted MC3T3-E1 cell survival and proliferation and enhanced ALP activity and calcium deposition compared with the PLGA/n-HA and PLGA/n-HA/VAN scaffolds. Additionally, the PLGA/n-HA/VAN+DOPA/rhBMP-2 scaffolds significantly facilitated new bone formation and inhibited bone infection in IBD rabbit models. The rabbits implanted with the PLGA/n-HA/VAN+DOPA/rhBMP-2 scaffolds exhibited normal heart, lung, and kidney histologies and normal serum biochemical indices, suggesting the safety of the scaffolds.

Conclusion: The 3D-printed PLGA/n-HA/VAN+DOPA/rhBMP-2 scaffolds exhibited both antibacterial and osteoinductive activities in IBD.

Keywords: infected bone defects, 3D printing, scaffolds, PLGA/n-HA, vancomycin, polydopamine, rhBMP-2, bone regeneration

Introduction

The reconstruction of bone defects caused by infection is a considerable clinical challenge.[1] The previous report has revealed that the rate of bone infection following open fractures ranges from 20% to 50%, which largely increases the

Received: 30 December 2024
Accepted: 28 April 2025
Published: 21 May 2025

therapeutic difficulty of bone defects and hinders the functional recovery of patients.[2] Pathogenic infections may severely affect the regeneration process of bone tissue despite its self-healing ability.[3] The conventional clinical management of infected bone defects (IBD) is divided into two phases: infection control through surgical debridement and systemic administration of antibiotics, and bone defect repair and local reconstruction through secondary grafting.[4] Currently, autografts and allografts are the most effective options for reconstructing localized bone defects.[5] Nevertheless, they exhibit inherent limitations, such as complex surgical technique, inadequate quantity, donor site morbidity, and immunological rejection.[6] Hence, the development of synthetic bone replacement materials with satisfactory osteogenic and antimicrobial activities for bone grafting has recently become a research hotspot.[7,8]

The three-dimensional (3D) printing technology has advanced considerably in the last decade and has now been extensively used in the field of medicine.[9] As the clinical demand for bone grafts continues to rise, a variety of scaffolds have been designed by utilizing 3D printing technology for bone repair and regeneration.[10] Natural polymers, which have favorable properties including biodegradability, biocompatibility, and ductility, have been widely used in scaffolds.[11] However, their application is limited by the presence of pathogenic impurities, the inability to accurately control the degradation rate, low mechanical properties, and poor stability.[12] Synthetic polymers overcome the defects of natural polymers to a certain extent, which have excellent mechanical properties, contain bone-promoting factors, and are highly biocompatible.[13] Poly(lactic-co-glycolic acid) (PLGA) is a synthetic co-polymer of poly(lactic acid) (PLA) and poly (glycolic acid) (PGA), which has advantages over pure PLA and PGA.[14] Nevertheless, PLGA is prone to elastic deformation and is also poorly osteoconductive, which limits the use of PLGA within bone tissue engineering.[15] To address these limitations, researchers have combined PLGA with bioceramics to prepare composite scaffolds.[16] Hydroxyapatite (HA) is a bioactive ceramic with a strong compositional similarity to bone and excellent osteoconductive and osteoinductive properties.[17] In recent years, composite scaffolds combined with synthetic polymers and HA have been created and applied in bone tissue engineering.[18,19] When contained in the composite scaffolds, synthetic polymers can balance the limitations of HA including slow degradation and inherent brittleness, and HA can improve tensile and compressive properties of scaffolds as well as promote cell and protein attachment to the scaffold material.[20,21] Existing studies have demonstrated that 3D-printed PLGA/nano-HA (n-HA) scaffolds can be used as ideal integrated bone grafting materials.[22]

The local prevention of infections following biomaterial implantation procedures is a challenge in the biomedical field, as such infections not only bring high treatment costs but also lead to morbidity and even mortality.[23] As the implantation of biomaterials will increase in the coming years, it is crucial to minimize the impact of these infections. Many different microorganisms are associated with skeletal infections, among which *Staphylococcus aureus* and coagulase-negative staphylococci (CoNS) (eg, *Staphylococcus epidermidis*) and *Streptococcus spp*. have been identified as the pathogenic bacteria of two-thirds of all skeletal infection cases.[24] These bacterial infections can destroy the balance between osteoblasts and osteoclasts, thereby inducing severe bone loss and destruction.[25] However, several strains will develop resistance to antibiotics and antimicrobial drugs and result in recurrence.[26] To solve this problem, porous biodegradable bone-related scaffolds are locally loaded with antibiotics to prevent or treat the infections after scaffold implantation.[27] Vancomycin is a promising antibiotic that exerts its antibacterial effect by impeding cell wall synthesis and inhibiting phospholipid and peptide production in the cell wall through interfering with peptidoglycan, an important component of bacterial cell wall structure.[28] Vancomycin is lethal to gram-positive bacilli and cocci commonly found in IBD, including *Staphylococcus aureus*, methicillin-resistant *Staphylococcus aureus*, and *Klebsiella pneumoniae*.[29] Nevertheless, the toxic side effects of systemic application of vancomycin cannot be ignored, such as respiratory depression, tinnitus, hearing loss, and renal damage.[30] Vancomycin has minimal adverse effects on osteoblasts and bone regeneration.[31] Local vancomycin delivery scaffolds can not only reduce the systemic toxicity and side effects of antibiotics but also release sufficient concentrations of local antimicrobial agents for preventive or therapeutic purposes.[32]

Bone regeneration is regulated by various bioactive agents, among which bone morphogenetic proteins (BMPs) are a group of highly conserved functional proteins with similar structures, belonging to the transforming growth factor-β (TGF-β) family.[33] BMPs can stimulate DNA synthesis and cell replication, thus inducing the directed differentiation of mesenchymal stem cells into osteoblasts, cartilage, and chondrocytes, and then promoting bone formation.[34] As powerful

osteoinductive factors, BMPs can act synergistically with bone tissue scaffolds to participate in bone regeneration.[35] In particular, BMP-2 is the most studied osteoinductive agent among the BMP family, whose osteogenic activity has been explored in the clinic.[36] As a result, BMP-2-based bone substitutes have been commercialized as an alternative to autologous grafts and approved by the Food and Drug Administration (FDA).[37] Multiple publications have pointed out that scaffolds loaded with BMP-2 effectively promote osteogenesis.[38,39] Nevertheless, many adverse side effects including ectopic cyst-like bone formation, inflammation, bone overgrowth, edema, and osteoclast activation have emerged with the increasing use of high-dose BMP-2 as well as its uncontrolled burst release from implants in bone disease treatment.[40,41] Considering the possible complications caused by BMP-2 in clinical use, selecting appropriate dosages, implementing supplemental factors, and employing carriers to improve the therapeutic efficacy of BMP-2 use and reduce the side effects are of great significance and have gained much attention.[42] To better control the release and bioactivity of BMP-2, there is an urgent need for a new delivery strategy that requires a lower dose of BMP-2 at the implantation site.[43] Nanohydrogels have garnered immense interest as potential carriers for delivering drugs, which can effectively control drug release and have good biocompatibility and safety.[44] Polydopamine (DOPA) hydrogel is a new kind of hydrogel material, which has broad application prospects in the field of nanomedicine.[45] A coating approach based on DOPA has been proposed to graft BMP-2 onto scaffolds without compromising the beneficial effects of the implanted materials and the biological activity of the growth factors.[46] DOPA has abundant catechol and amine groups, making covalent coupling with bioactive molecules containing primary amine or thiol groups.[47] Accordingly, DOPA coating has been used to immobilize growth factors on substrates.[47] In addition, the superior adhesive properties of mussel-inspired material DOPA can convert polymer substrates from hydrophobic to hydrophilic, thereby modifying the poor surface properties of tissue-engineered polymer scaffolds.[48] Even though many synthetic scaffolds have been developed and their beneficial effects on IBD have been studied, few scaffolds simultaneously encapsulated with both antibiotics and osteoinductive agents have been designed.

In this study, the 3D-printed PLGA/n-HA scaffolds were grafted with vancomycin and then coated with rhBMP-2 via DOPA chemistry to create the composite scaffolds. The characterization, cytocompatibility, and osteoconductive properties of the composite scaffolds were assessed in vitro. Furthermore, the composite scaffolds were implanted into the defect sites of rabbit radius to explore their effects on bone regeneration and bone infection in vivo.

Materials and Methods

Fabrication of the 3D-Printed PLGA/n-HA Scaffolds

The PLGA/n-HA scaffolds were fabricated layer-by-layer using a 3D-Bioplotter machine (3D-Bioplotter, Envision TEC GmbH, Germany) under the guidance of supporting computer workstations as described elsewhere.[22,49] PLGA particles (molecular weight = 200,000 Da; LA/GA = 75/25) were purchased from Jinan Daigang Biomaterial Co., Ltd. (Shandong, China). Nano-hydroxyapatite (n-HA; particle size≈50 μm; #KL811001) was obtained from KALANG (Shanghai, China). Briefly, PLGA particles were dissolved in 1,4-dioxane to prepare a homogeneous solution, which was then added with n-HA powders and sufficiently mixed under continuous stirring for 12 h to form a uniform paste. The PLGA/n-HA composite scaffolds were composed of 80% PLGA and 20% n-HA. A cubic scaffold model was created on the slicing software and then loaded into the 3D drawing system. The mixture of PLGA and n-HA was melted in a heating dispenser at 150 °C melting temperature and extruded from computer-driven dispensers through the nozzle. The detailed parameters were controlled by computer and set as follows: nozzle temperature 150 °C, nozzle inner diameter 0.2 mm, extrusion speed 18 mm/sec, extrusion pressure 0.11 MPa. Afterwards, the 3D-printed PLGA/n-HA scaffolds with porous stereo-structures (diameter: 6 mm; height: 9 mm) were manufactured layer-by-layer. The resulting scaffolds (filament diameter: 0.55 mm; pore size: 400 μm; porosity: 45%) were sterilized by ultraviolet radiation for 24 h and dried under vacuum at 37 °C for 48 h.

Vancomycin Loading on the PLGA/n-HA Scaffolds

After fabrication, the PLGA/n-HA scaffolds were loaded with the antibiotic vancomycin (vancomycin hydrochloride; lyophilized powder, #CB939; Warbio, Nanjing, China) through dip coating as previously described.[50] In short, the

 https://doi.org/10.2147/IJN.S514978

scaffolds were immersed in vancomycin solution (1 mL, 42.5 mg/mL) in ultrapure water to allow the penetration of the solution into the scaffold pores. This process was performed in a vacuum chamber and lasted for 1 h. Finally, the vancomycin-loaded scaffolds (PLGA/n-HA/VAN) were dried for 24 h at 37 °C.

Preparation of DOPA-Coated PLGA/n-HA/VAN Scaffolds and rhBMP-2 Grafting

Dopamine hydrochloride (#D103111) and Escherichia coli-expressed human recombinant BMP-2 (rhBMP-2; #120-02) were bought from Aladdin (Shanghai, China) and PeproTech (Rocky Hill, NJ, USA), respectively. The PLGA/n-HA/VAN scaffolds prepared as described above were immersed for 2 h at room temperature (RT) in dopamine hydrochloride solution (2 mg/mL in 10 mm of Tris buffer, pH 8.5). Subsequently, the DOPA-coated PLGA/n-HA scaffolds were washed three times with fresh deionized water, dried under nitrogen gas, and immersed in rhBMP-2 solution (500 ng/mL in 10 mm of Tris buffer, pH 8.5).[51] After 24 h stirring at RT, rhBMP-2 was directly grafted and immobilized, followed by three times washing with fresh deionized water. The DOPA-coated and rhBMP-2-grafted PLGA/n-HA/VAN scaffolds were abbreviated as PLGA/n-HA/VAN + DOPA/rhBMP-2.

Scaffold Characterization

The 3D-printed PLGA/n-HA scaffolds were observed under an optical microscope (Eclipse E200, Nikon, Tokyo, Japan) and photographed. Subsequently, the scaffolds were dehydrated through an ethanol gradient and dried by critical point drying. To estimate the water absorption of the scaffolds, the dried scaffolds were first weighed using a precision balance (BSA 224S-CW Sartorius, USA) and then immersed for 24 h at 37 °C in a 10 mL vial containing distilled water. After removing the surface water with a Kim wipe, the mass of scaffolds after water absorption was recorded. The water uptake ratio was calculated according to the following formula: Water uptake (%) = $[(W_{after}\text{-}W_{before})/W_{before}] \times 100$.

A water contact angle test was conducted to assess the hydrophilicity of the scaffolds by using a contact angle goniometer (OCA15EC, DataPhysics, Filderstadt, Germany). In brief, the scaffolds were placed on the testing plate, and deionized water (20 μL) was dropped onto the scaffold surface. Thereafter, a high-resolution camera was used to capture the images of the droplets, and the angle between the scaffold surface and the droplet was detected. The measurement of each scaffold was repeated in triplicate and the average water contact angle was finally calculated.

The mechanical properties (including the compressive strength and tensile strength) of the prepared PLGA/n-HA, PLGA/n-HA/VAN, and PLGA/n-HA/VAN + DOPA/rhBMP-2 scaffolds were analyzed by using a mechanical test machine (Instron 5567, Norwood, MA, USA) at a crosshead speed of 1 mm/min.

The surface chemistry of the composite scaffolds was identified through the x-ray photoelectron spectroscopy (XPS) analysis by using an XPS PHI5000 VersaProbe II (ULVAC-PHI, Japan). The aluminum k-α X-ray line (energy: 1.4866 keV; X-ray spot size: 400 μm) was used as the probe to acquire both survey and regional high-resolution spectra at each scaffold. The data for survey spectra were collected at a pass energy of 200 eV, with 5 scans in 1 eV step. The data for high-resolution spectra of C 1s, N 1s, and O 1s photoelectron lines were obtained at a pass energy of 50 eV, with 10 scans in 0.1 eV steps. During the data acquisition, the pressure in the analysis chamber was approximately 10^{-9} Torr. PHI MultiPak XPS software was used along with Gaussian-Lorentzian lines to fit the XPS spectra. The background from the spectrum was removed using a Shirley-type background before the peak fitting.

Detection of Drug Release by Scaffolds in vitro

The PLGA/n-HA/VAN and PLGA/n-HA/VAN+DOPA/rhBMP2 scaffolds were transferred to a 10 mL centrifugation tube containing 4 mL of phosphate-buffered solution (PBS; pH: 7.4) and placed in a shaker (100 rpm) under a constant temperature (37 °C) for 30 days. Then, 4 mL PBS solution was sampled every 24 h for testing, and replaced with fresh amounts (4 mL) of PBS. The collected solution was characterized by high-performance liquid chromatography (HPLC) on a Hitachi L-2200 Multisolvent Delivery System. The mobile phase employed for vancomycin separation contained 0.01 mol heptanesulfonic acid and acetonitrile. The absorbance was monitored at 280 nm with a flow rate of 1.4 mL/min to detect precise amounts of the released vancomycin. The amount of BMP-2 in the supernatant was measured using a commercialized enzyme-linked immunosorbent assay (ELISA) kit (#EHC172.96; NEOBIOSCIENCE, Shenzhen, China) following the manufacturers' instructions. After adding a colorimetric substrate solution, the absorbance at 450

nm was measured using a PowerWave HT microplate spectrophotometer (BioTek, Winooski, VT, USA). Finally, the standard elution curves showing the cumulative release of vancomycin and BMP-2 in the composite scaffolds were respectively generated.

In vitro Cytocompatibility Assay

Mouse embryonic osteoblast MC3T3-E1 cells (#KBR-JY30823; Keborui Bio, Shanghai, China) were cultured in MEM Eagles with Earle's Balanced Salts (MEM/EBSS; #SH30024.01B, Solarbio, Beijing, China) supplemented with 10% fetal bovine serum (FBS; #abs972; Absin, Shanghai, China) and 1% penicillin-streptomycin (#60162ES76; Yeason, Shanghai, China) in a humidified atmosphere (5% CO_2, 37 °C).

The survival of MC3T3-E1 cells on the composite scaffolds was determined using the live/dead cell staining kit (#ab65470; Abcam, Shanghai, China). Briefly, 5×10^3 MC3T3-E1 cells were seeded with scaffolds into each well of 24-well plates at 37 °C for 24 h. After co-culturing for 1 and 3 days, the culture medium was discarded and the cells were washed twice with PBS, followed by 20 min incubation at 37 °C in the dark with 200 μL of live/dead reagent containing 4 μM Calcein AM and 8 μM PI. Afterwards, the residual staining solution was removed after the cells were washed twice with PBS. Under fluorescence microscopy (Leica, Germany), green-stained and red-stained cells represented live cells and dead cells, respectively.

For the Cell Counting Kit-8 (CCK-8) assay, MC3T3-E1 cells (5×10^3 cells/well) were seeded with scaffolds into 24-well plates, and the plates were incubated at 37 °C for 24 h. After co-culturing for 1, 3, and 7 days,10 μL of CCK-8 working solution (#HY-K0301; MedChemExpress, Shanghai, China) was added to each well and incubated for 2 h. The optical density value of each well at 450 nm was measured using a full-wavelength microplate reader (Multiskan GO, Thermo Fisher Scientific, USA).

In vitro Osteogenic Effects

To explore the influence of the composite scaffolds on osteogenic differentiation, MC3T3-E1 cells were inoculated (5×10^4 cells/well) with scaffolds into 6-well plates supplemented with osteogenic induction medium (#MGY8024; MesGen Biotech, Shanghai, China). After a 14-day incubation period, alkaline phosphatase (ALP) staining and activity analysis were conducted. For ALP staining, the cells were washed three times with PBS, fixed for 15 min with 4% paraformaldehyde, and treated with BCIP/NBT staining working solution (#mlsw-3162; MLBio, Shanghai, China). The cells were imaged by microscopy following co-incubation for 1 h and protected from light at 25 °C. The enzyme activity was detected using an ALP activity kit (#abs580003; Absin). The well plate was added with RIPA lysis buffer (#C1053; Applygen, Beijing, China), and the supernatant was harvested. Subsequently, the sample was added with the chromogenic substrate and diethanolamine, followed by another 30 min incubation at 37 °C. Finally, the ALP activity was determined by examining the absorbance at 405 nm by employing a microplate reader.

MC3T3-E1 cells were seeded (5×10^4 cells/well) with scaffolds in 6-well plates. After a 21-day cell culture with the osteogenic induction medium, Alizarin Red S (ARS) staining was performed to study cell mineralization. Briefly, the cells were rinsed thrice with PBS, and 4% paraformaldehyde was added for 15 min for cell fixation. Each well was added with 2% alizarin red solution (#C0138; Beyotime, Shanghai, China), and the cells were incubated at 37 °C for 30 min in the dark. Finally, the staining solution was discarded and cells were washed with PBS for three times. The mineralized nodules were observed under an inverted microscope (Leica, Germany).

Establishment of IBD Model in Rabbits and Scaffold Implantation

The healthy New Zealand white rabbits with mature skeletons (half male and half female; 6 months old; 3.5 ± 0.3 kg) provided by Vital River Inc. (Beijing, China) were used in our study. All experiments were performed in an open system laboratory (humidity: 40–60%; temperature: 22–24 °C). All of the experimental procedures followed National Institutes of Health (NIH)-mandated guidelines for animal welfare and were approved by the Animal Ethics Committee of First People's Hospital of Kashgar. Thirty rabbits were assigned to the PLGA/n-HA, PLGA/n-HA/VAN, and PLGA/n-HA/VAN+DOPA/rhBMP2 groups (n=10 per group) according to the randomization principle. The establishment of rabbit IBD models followed the method described previously.[52,53] In short, the rabbits were anesthetized by the intramuscular

injection of 3% (w/v) sodium pentobarbital (50 mg/kg). Then, the rabbits were placed on the operating table in a supine position and well-fixed. The right radius was chosen as the modeling site. After shaving, disinfection was performed by using iodophor, and sterile tablecloths were set. We made a 20 mm longitudinal incision along the inner side of the forearm to expose the middle segment of the radius. A 6 mm segmental defect was then created in the middle radius using a miniature orthopedic pendulum saw according to the length of the implant. Simultaneously, thermal damage to the bone was prevented through continuous PBS irrigation. The PLGA/n-HA, PLGA/n-HA/VAN, and PLGA/n-HA/VAN +DOPA/rhBMP2 scaffolds were contaminated with the prepared *Staphylococcus aureus* in 2 mL PBS (1×10^6 CFUs/mL) for 10 min to ensure $1.3 \pm 0.2 \times 10^4$ CFUs of bacteria attached on the surface of each scaffold. Thereafter, the prepared scaffolds were respectively inserted into the bone defect region. The wound was meticulously sutured in a layered manner. All rabbits were individually caged, irradiated with a baking lamp to maintain body temperature, and carefully observed until full recovery. Bone infection persisted locally during the follow-up period in all groups, and no post-operative antibiotics were given. Samples of the surgical site were harvested at 12 weeks after surgery for further investigation.

Micro-CT Analysis

At 12 weeks postoperatively, the surgical sites from three rabbits in each group were collected, soaked for 48 h in 4% paraformaldehyde for fixation, and rinsed overnight with running water for micro-CT scan to evaluate new bone formation. The samples were scanned using a Skyscan 1172 micro-CT scanner (Bruker micro-CT, Kontich, Belgium) at an energy of 88 kV, an intensity of 100 μA intensity, and a pixel resolution of 8.665 μm. The reconstructed 3D images were obtained using the CTvox software (Bruker, Kontich, Belgium), and the bone volume fraction (BV/TV; bone volume to total volume ratio) was calculated based on these images to assess bone structure.

Histological Staining

After the rabbits were sacrificed at week 12 after surgery, the radius samples (approximately 2 cm above and below the scaffold) were cut with the micro-pendulum saw, and the attached soft tissues of the radius were scraped off. The samples were fixed for 48 h in a 10% formalin solution (#QYK-15110; Qiyuan, Shanghai, China)), decalcified using 10% ethylenediaminetetraacetic acid (EDTA; pH: 7.4; #abs9223; Absin) for 1 month, rinsed with running water, immersed in ethanol concentrations of 70%, 80%, and 90% (soaking time: 2 h/concentration) for dehydration, cleared in xylene, and embedded in paraffin. The paraffin-embedded tissues were sectioned at 5 μm thickness and then stained using hematoxylin and eosin (H&E) staining kit (#C0105S; Beyotime) to evaluate the morphology and microstructure of bones and using Masson's trichrome staining kit (#C0189; Beyotime) to detect collagen deposition in bone tissues. The stained sections were observed under a digital microscope (DSX 500; Olympus, Tokyo, Japan), and the surface area of new bones was quantitatively analyzed using ImageJ software (NIH, USA).

Immunohistochemical Staining

The paraffin-embedded radial tissues of rabbits were prepared and cut into 5-μm-slices as described above in histological staining. The slices were deparaffinized and hydrated in ethanol with decreasing concentrations. To block endogenous peroxidase, the samples were incubated for 30 min at RT with 3% hydrogen peroxide in methanol solution. The slides were then boiled in a steamer immersed in citrate buffer (pH 6.0) for 10 min to achieve antigen retrieval. After 1 h of non-specific binding blockage with 10% goat serum, the sections were incubated with the primary antibodies against RUNX2 (#A2851; 1:100; ABclonal, Wuhan, China) and OCN (#HZK-11654; 1:100; Huzhen, Shanghai, China) at 4 °C overnight and washed three times with PBS. A horseradish peroxidase-conjugated secondary antibody (#AS014; 1:100; ABclonal) was added for a further 30 min incubation at RT, followed by three PBS washes. Then, the slides were stained for 10 min at 37 °C with aminoethylcarbazole with 3,3′-diaminobenzidine tetrahydrochloride (DAB; #36201ES03; Yeason) as a chromogen. After counterstaining for 3 min at RT with Mayer's hematoxylin (#G1080; Solarbio), the sections were visualized under an Olympus digital microscope. Semi-quantitative analysis of the immunohistochemical staining images was performed using ImageJ software.

Microbiological Assessment

At 12 weeks after surgery, the implanted scaffolds and about 5 mm of the bones at each end of the scaffolds were removed from three randomly selected rabbits from each group under aseptic conditions and subjected to the plate rolling experiment to evaluate bacteria viability at the surgical site.[54] The collected samples were snap-frozen in liquid nitrogen, placed in sterile grinding dishes, and ground into powder. Thereafter, the scaffold and tissue powders were put into a sterile tube, vortexed for 2 min in 2 mL of PBS, and fully mixed. After centrifugation at 10,000 g for 15 sec, the supernatants were withdrawn for serial (10-fold) dilutions, smeared on the bacterial culture plates, and incubated at 36 °C for 24 h. Finally, the samples were analyzed for CFUs/bone and CFUs/scaffold.

In vivo Safety Evaluation of the Composite Scaffolds

The heart, liver, and kidney tissues of rabbits were taken for H&E staining at 12 weeks post-surgery to observe toxic reactions. To measure the levels of several biochemical indices, blood samples were drawn from the tail vein of rabbits and centrifuged for 5 min at 8000 g to obtain the serum, which was stored in a −80 °C freezer. The levels of aspartate transaminase (AST; #abs580004; Absin), alanine transaminase (ALT; #abs580002; Absin), blood urea nitrogen (BUN; #abs580197; Absin), and creatine kinase (CK; #abs580044; Absin) in the serum were examined using the corresponding assay kits as per the manufacturer's instructions.

Statistical Analysis

At least three samples were included in every group for all in vitro experiments in this study. Two-group and multi-group comparisons were compared using Student's *t*-test and one-way analysis of variance coupled with Tukey's post-test, with $P < 0.05$ regarded as statistically significant. All data were analyzed using SPSS 24.0 statistical software and are represented as the mean ± standard deviation.

Results

Morphology of 3D Printed Scaffolds

As shown in Figure 1A and B, the cylindrical scaffolds fabricated by 3D printing technology exhibited a regular morphology and the pore diameter of the macroporous morphology was 400 μm.

Analysis of the Hydrophilicity and Surface Chemical Composition of 3D Printed Scaffolds

The PLGA/n-HA scaffold modified with DOPA/rhBMP-2 was subjected to the water uptake experiment, whose results revealed that the water absorption of unmodified PLGA/n-HA was very low within 60 sec whereas the DOPA/rhBMP-2-modified PLGA/n-HA could absorb water rapidly. Moreover, it was observed that the PLGA/n-HA+DOPA/rhBMP-2 sank in the cell culture medium, while the PLGA/n-HA floated on the surface of the medium (Figure 2A). The water

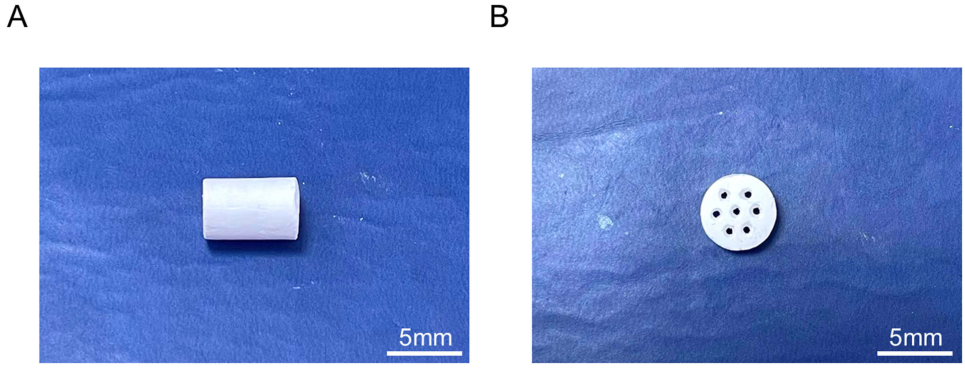

Figure 1 Morphological characterization of the 3D printed scaffolds. (**A** and **B**) The side and top view of the PLGA scaffolds.

https://doi.org/10.2147/IJN.S514978

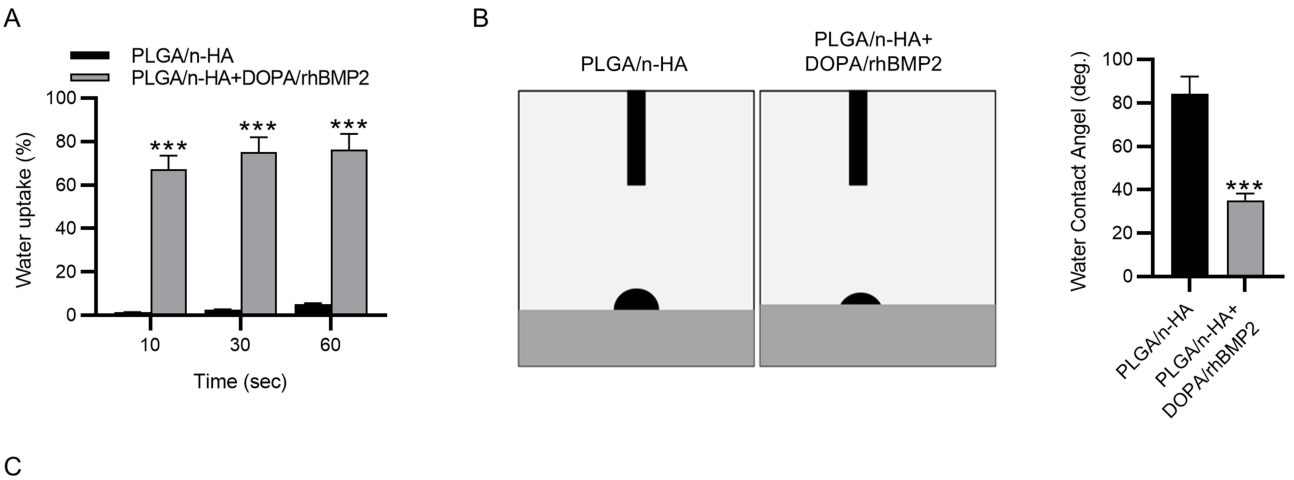

C

	C	N	O
PLGA/n-HA	65.54	0	34.46
PLGA/n-HA+DOPA/rhBMP2	60.47	3.71	35.82

Figure 2 Hydrophilicity and surface chemical composition of the 3D printed scaffolds. (**A**) Water uptake rate, (**B**) water contact angle, and (**C**) surface chemical composition of PLGA/n-HA and PLGA/n-HA+DOPA/rhBMP-2. ***p < 0.001.

contact angle test further confirmed these results. As revealed in Figure 2B, the PLGA/n-HA+DOPA/rhBMP-2 showed a significant decrease in the water contact angle (35.11°±3.14) compared to the control bare PLGA/n-HA (84.15°±8.03), suggesting that the surface modification with DOPA/rhBMP-2 significantly increased the hydrophilicity of PLGA/n-HA. This phenomenon was caused by hydrophilic DOPA.[55] Next, XPS analysis was performed against the bare and modified PLGA/n-HA to validate the surface chemical element composition of the scaffolds. The increase in N1s content in the PLGA/n-HA+DOPA/rhBMP-2 attributed to the introduction of amine groups by the DOPA coating (Figure 2C), which indicated that DOPA was well coated on the PLGD/n-HA scaffolds and allowed rhBMP-2 to subsequently attach and effectively immobilize on the PLGD/n-HA scaffolds.

Mechanical Properties and in vitro Drug Release of the Composite Scaffolds

Scaffolds used for bone implantation need to withstand certain mechanical loads during normal use, so the materials used should have good mechanical strength to provide stable support and protection for injured or missing bones. The mechanical test results (compressive strength and tensile strength) in Figure 3A and B illustrated that the mechanical properties of the three scaffolds all appeared similar to those of human natural cancellous bones.[56] We also examined the accumulated release of vancomycin from the composite scaffolds. The drug-elution profiles of the PLGA/n-HA/VAN and PLGA/n-HA/VAN+DOPA/rhBMP-2 scaffolds showed similar trends, with a cumulative drug-elution rate close to 90% at day 30 (Figure 3C). In addition, the continuous and regular elution of BMP-2 from the PLGA/n-HA/VAN+DOPA/rhBMP-2 scaffolds was observed, with almost complete release at day 25 (Figure 3D).

Biocompatibility and Osteoconductive Properties of the Composite Scaffolds

To determine the biocompatibility of the composite scaffolds, MC3T3-E1 cells were respectively seeded onto the PLGA/n-HA, PLGA/n-HA/VAN, and PLGA/n-HA/VAN+DOPA/rhBMP-2 scaffolds for co-culture and the effects of the composite scaffolds on cell viability and proliferation were evaluated by performing live/dead cell staining and CCK-8 assays. As shown in Figure 4A, the number of living cells was remarkably higher on day 3 than on day 1 in all three groups. Similarly, CCK-8 assay depicted that excellent cell growth was observed from days 1–7 in all groups. There was no statistically significant difference in cell number between the PLGA/n-HA and PLGA/n-HA/VAN groups. However, compared with these two groups, the PLGA/n-HA/VAN+DOPA/rhBMP-2 group presented markedly increased cell

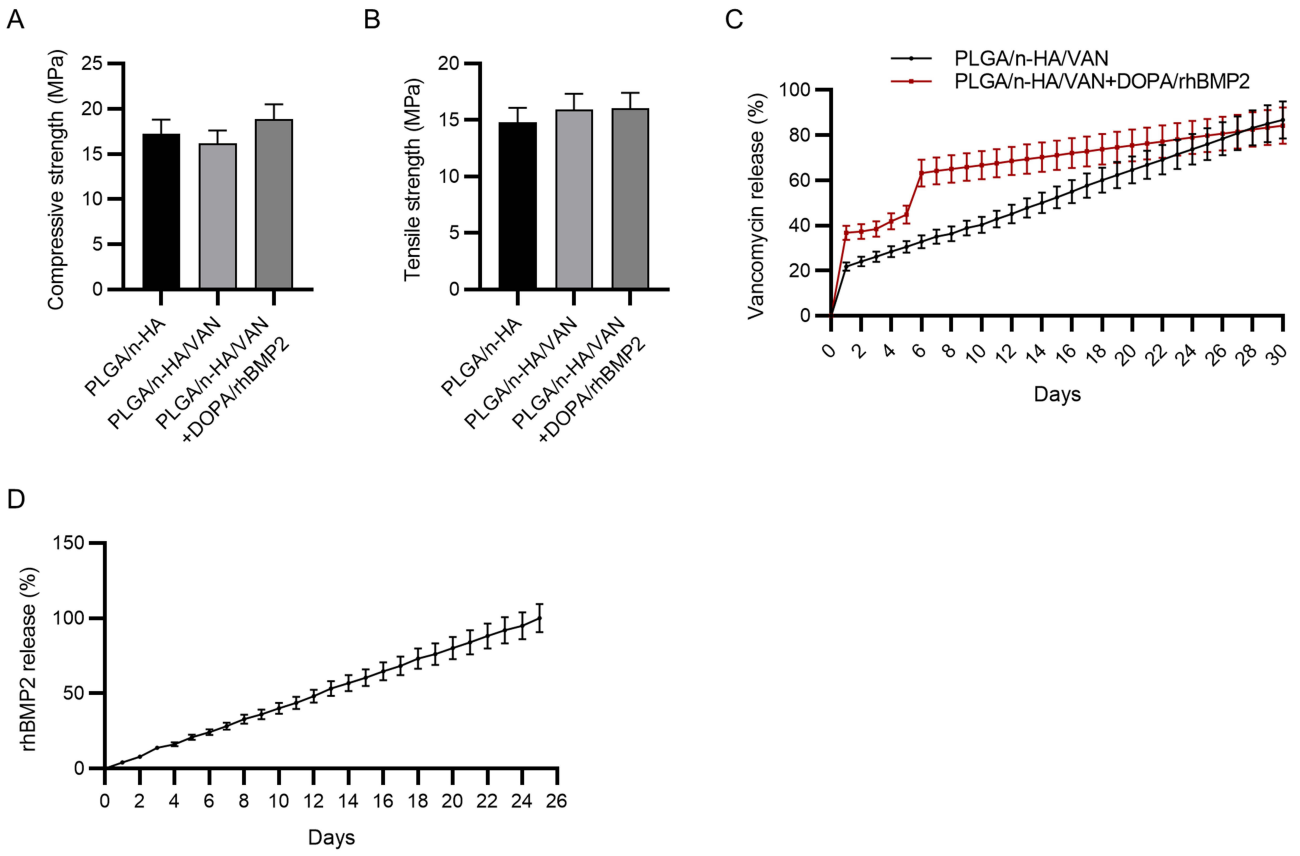

Figure 3 Mechanical properties and in vitro drug release of the composite scaffolds. (**A** and **B**) Mechanical characteristics (compressive strength and tensile strength) of the composite PLGA/n-HA, PLGA/n-HA/VAN, and PLGA/n-HA/VAN+DOPA/rhBMP-2 scaffolds. (**C**) The accumulated release of vancomycin from the composite PLGA/n-HA/VAN and PLGA/n-HA/VAN+DOPA/rhBMP-2 scaffolds in vitro. (**D**) The accumulated release of BMP2 from the composite PLGA/n-HA/VAN+DOPA/rhBMP-2 scaffolds in vitro.

numbers within 7 days (Figure 4B). These two assays suggest that three composite scaffolds are beneficial for MC3T3-E1 cell growth, with the PLGA/n-HA/VAN+DOPA/rhBMP-2 scaffold exhibiting better favorable effects. To investigate the osteogenic effects of the composite scaffolds in MC3T3-E1 cells, ALP staining and ALP activity assay were conducted after osteogenesis induction. ALP staining showed a small number of ALP-positive cells in MC3T3-E1 cells cultured on PLGA/n-HA and PLGA/n-HA/VAN scaffolds. In contrast, more significant ALP staining was observed in MC3T3-E1 cells cultured on PLGA/n-HA/VAN+DOPA/rhBMP-2 scaffolds compared with the other two scaffolds (Figure 4C). The results of ALP activity assay were consistent with those of ALP staining, which manifested that MC3T3-E1 cells cultured on the surface of PLGA/n-HA/VAN+DOPA/rhBMP-2 scaffolds had notably higher ALP activity than those cultured on the surface of other two scaffolds (Figure 4D). Subsequently, we conducted ARS staining in MC3T3-E1 cells to estimate the influence of the composite scaffolds on calcium deposition, which is another feature of osteoblastic differentiation. As observed in Figure 4E, red calcium nodules in the PLGA/n-HA/VAN+DOPA/rhBMP-2 scaffolds were stained more prominently and in a larger area than the other two scaffolds. Therefore, the PLGA/n-HA/VAN+DOPA/rhBMP-2 scaffolds exhibited better promotive effects on osteoblastic differentiation than the PLGA/n-HA and PLGA/n-HA/VAN scaffolds.

Establishment of an Infected Bone Defect Model and Scaffold Implantation in the Radius

Next, we established a rabbit model of infected bone defects of the radius to investigate the therapeutic effects of the composite scaffolds on bone remodeling in vivo. As revealed in Figure 5A–C, the middle radius of the rabbits was exposed and the length of the osteotomy was determined as 6 mm according to the length of the scaffold. The scaffold

https://doi.org/10.2147/IJN.S514978

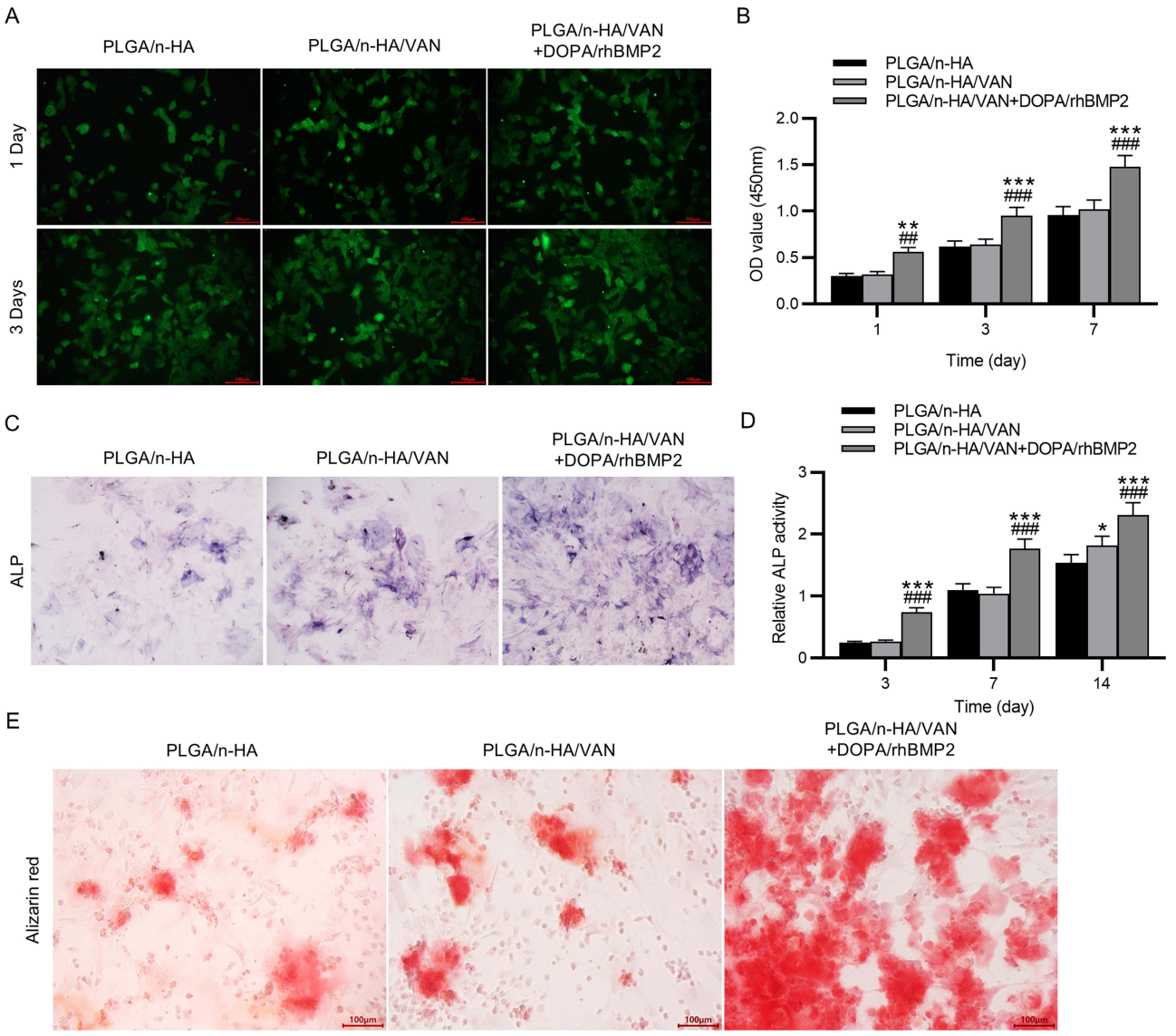

Figure 4 Biocompatibility and osteoconductive properties of the composite scaffolds. MC3T3-E1 cells were respectively seeded onto the surface of the PLGA/n-HA, PLGA/n-HA/VAN, and PLGA/n-HA/VAN+DOPA/rhBMP-2 scaffolds for co-culture. (**A**) Assessment of MC3T3-E1 cell viability on days 1 and 3 through live/dead cell staining. The live and dead cells were stained green and red, respectively. (**B**) Evaluation of MC3T3-E1 cell proliferation within 7 days by CCK-8 assay. (**C**) Representative ALP staining images of MC3T3-E1 cells from each group. (**D**) Detection of ALP activity in MC3T3-E1 cells. (**E**) Representative ALP staining images showing the deposition of calcium (stained red) in MC3T3-E1 cells. *$p < 0.05$, **$p < 0.01$, ***$p < 0.001$ versus the PLGA/n-HA group; $^{\#\#}p < 0.01$, $^{\#\#\#}p < 0.001$ versus the PLGA/n-HA/VAN group.

was then tightly embedded into the defect area. Since the ulna is the major bone of the rabbit's upper limb, the radius was chosen as the modeling area that would neither interfere with the rabbit's normal activity nor require the use of other metallic implants to minimize artifactual interference in imaging examination. Besides, the rabbits are unable to repair bone defects exceeding 1.5 times the backbone diameter. The length of the radial defect was set at 6 mm considering that the radius diameter in rabbits is typically 3 mm.

Micro-CT Analysis of New Bone Formation in IBD Rabbit Models

At 12 weeks after the scaffold implantation, the healing of the bone defect was evaluated through Micro-CT analysis (Figure 6A). There were obvious osteomyelitis and irregular bone formation at the defect site in both PLGA/n-HA and PLGA/n-HA/VAN groups, but no union was observed at the defect area. No infection signs were discovered in the PLGA/n-HA/VAN+DOPA/rhBMP-2 group, with new bones growing into the scaffold and forming a continuous healing bone at the site of the bone defect. To determine new bone formation in the areas of scaffold implantation in all three groups, we further

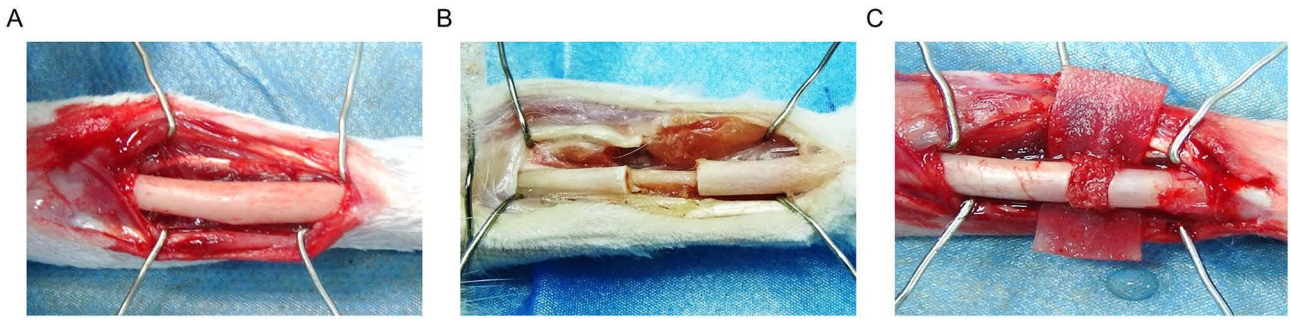

Figure 5 Establishment of an infected bone defect model and scaffold implantation in the radius. (**A**) The exposed middle radius of the rabbits. (**B**) The length of radius defects was determined based on the scaffold length. (**C**) The scaffold implantation into the radius defect area after osteotomy.

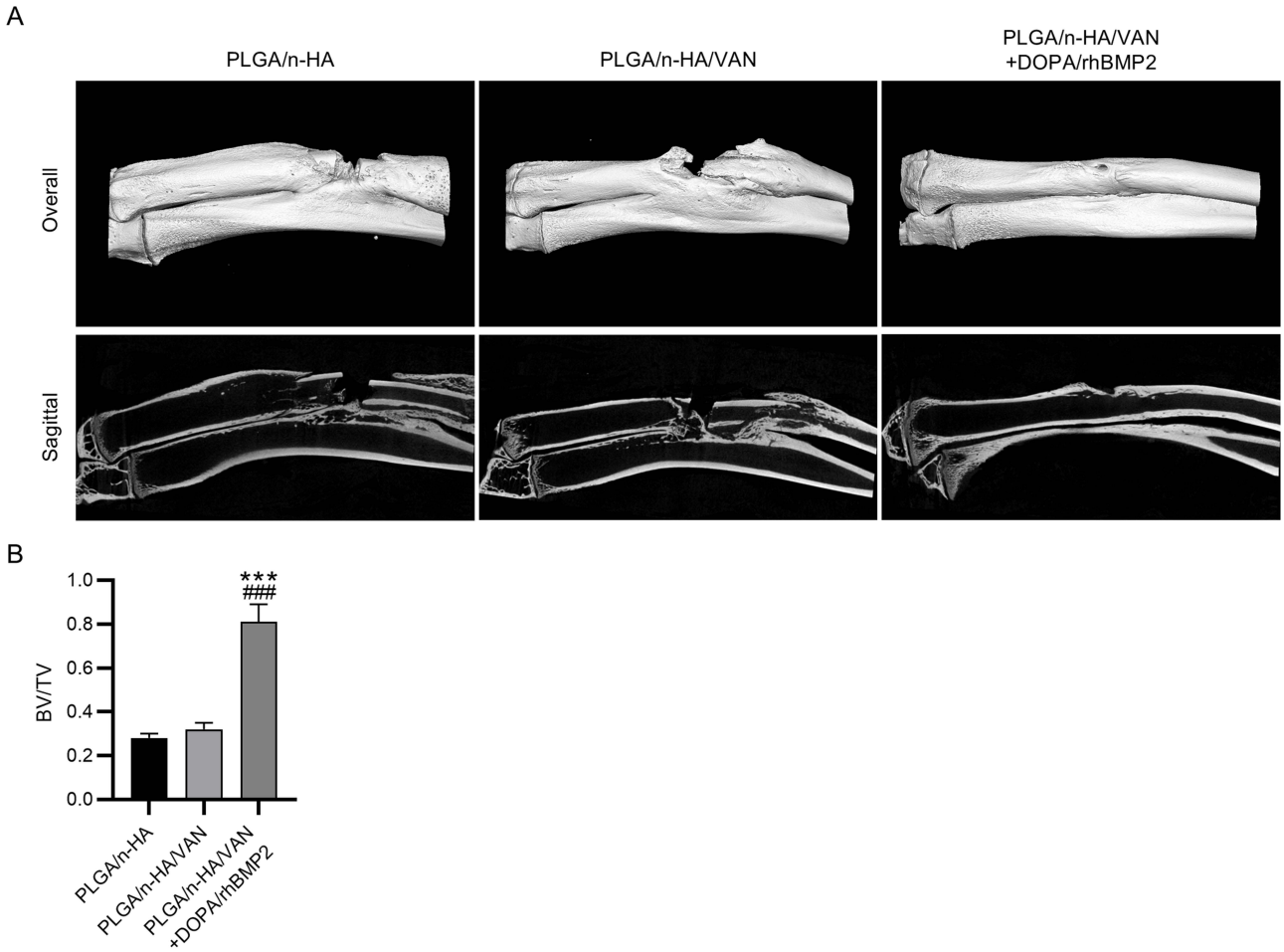

Figure 6 Micro-CT analysis of new bone formation in IBD rabbit models. (**A**) Micro-CT images of the rabbit's upper limb implanted with the scaffolds at week 12 after operation. (**B**) Analysis results of bone volume/total volume (BV/TV) in the defect area. ***$p < 0.001$ versus the PLGA/n-HA group; ###$p < 0.001$ versus the PLGA/n-HA/VAN group.

performed morphological measurements on the lesion areas. The BV/TV of the PLGA/n-HA/VAN+DOPA/rhBMP-2 group was considerably higher than that of the PLGA/n-HA and PLGA/n-HA/VAN groups (Figure 6B).

Histological Examination

Next, the histopathological changes in the adjacent bone interface area and scaffold sections of rabbits at 12 weeks after surgery were observed through H&E and Mason staining (Figure 7A). H&E staining demonstrated that many pus cells

https://doi.org/10.2147/IJN.S514978

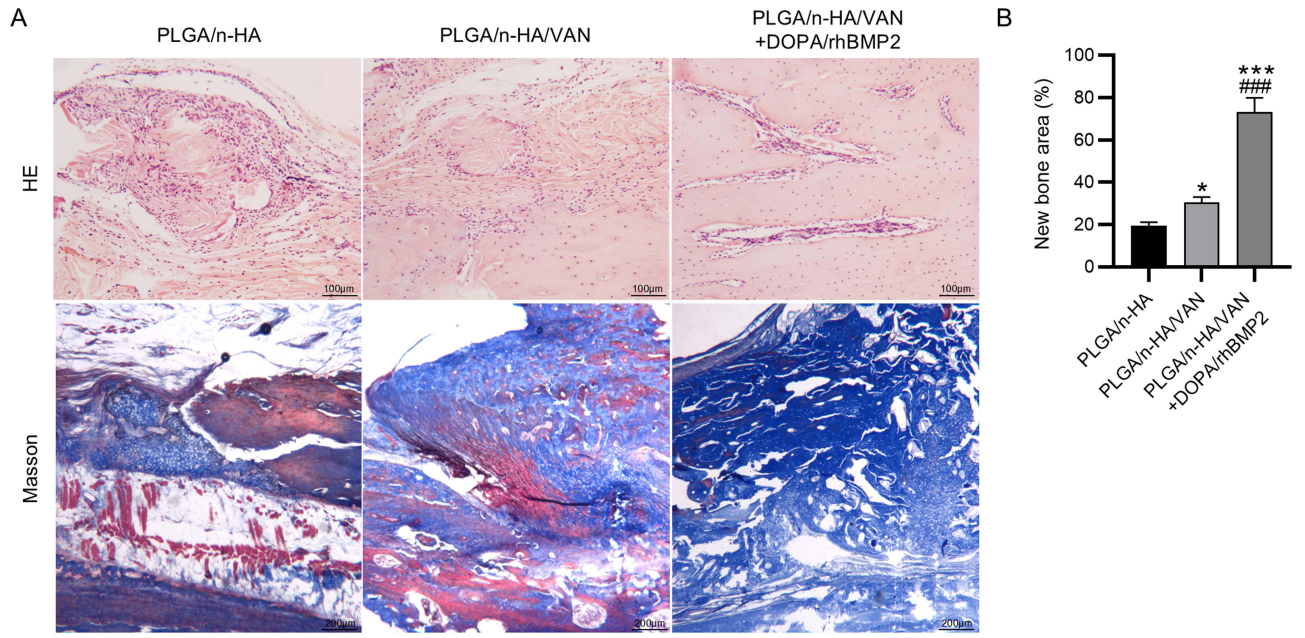

Figure 7 Histological examination. (**A**) Representative H&E staining (upper panels) and Masson staining (lower panels) images showing bone histopathological changes and collagen deposition at the interface between the bone and scaffold 12 weeks after surgery. (**B**) Quantification of new bone areas at 12 weeks based on the results of histological staining. *$p < 0.05$, ***$p < 0.001$ versus the PLGA/n-HA group; ###$p < 0.001$ versus the PLGA/n-HA/VAN group.

were immersed in the bone tissues in the PLGA/n-HA group, accompanied by partial dead bone in the junction area, bone destruction and absorption, and a few reactive new bones at the margin, which suggested that the bacteria proliferated and caused chronic osteomyelitis. No pus cell aggregation was noted in the PLGA/n-HA/VAN group, with limited formation of new bone. In contrast, in the PLGA/n-HA/VAN+DOPA/rhBMP-2 group, a large amount of new bone was formed and passed through the junction area, and the trabeculae displayed higher integrity, regularity, and density. The maturity of collagen in the bone tissues was evaluated through Masson staining, through which we found that the PLGA/n-HA/VAN+DOPA/rhBMP-2 group showed an increase in regenerated bone tissues and good regeneration of new bone at 12 weeks postoperatively. Although there was new bone formation in the PLGA/n-HA/VAN group, the amount of new bone was dramatically lower than in the PLGA/n-HA/VAN+DOPA/rhBMP-2 group. Image J software was used to quantify the new bone area in the stained section. The data indicated that the PLGA/n-HA/VAN+DOPA/rhBMP-2 group had distinctly larger new bone area than the PLGA/n-HA and PLGA/n-HA/VAN groups (Figure 7B). These results demonstrate that the PLGA/n-HA/VAN+DOPA/rhBMP-2 scaffolds can better promote new bone formation and collagen production than the other two scaffolds.

Immunohistochemical Staining of RUNX2 and OCN

Osteogenesis-related proteins RUNX2 and OCN were used as indicators of bone formation, whose expression in bone tissues of IBD rabbit models after scaffold implantation was further confirmed through immunohistochemistry analysis. As illustrated in Figure 8, the number of RUNX2-positive and OCN-positive cells was notably higher in the PLGA/n-HA/VAN+DOPA/rhBMP-2 group than in the PLGA/n-HA and PLGA/n-HA/VAN groups. This suggested that implantation with the PLGA/n-HA/VAN+DOPA/rhBMP-2 scaffolds significantly enhanced the expression of osteogenesis-related proteins in IBD rabbit models compared with the other two scaffolds.

Evaluation of Antibacterial Properties of Scaffolds in vivo

At week 12 post-operatively, the implanted scaffolds and the bone tissues at the ends of the scaffolds were respectively obtained from three random rabbits in each group, and the spreading plate method was then used for quantitative

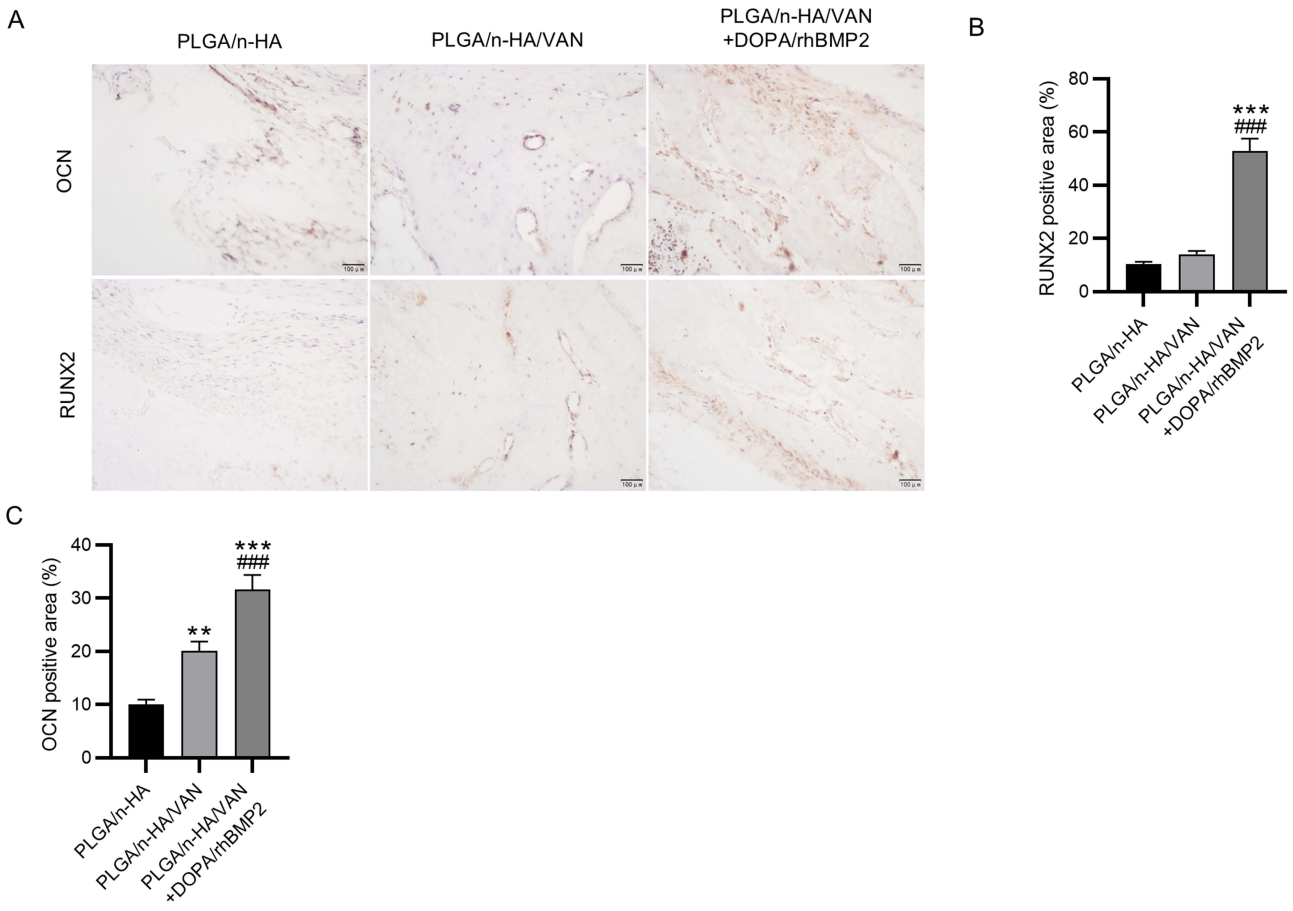

Figure 8 Immunohistochemical analysis of osteogenesis-related proteins in IBD rabbit models. (**A**) Representative immunohistochemical staining images showing RUNX2 and OCN expression in bone tissues of IBD rabbit models after scaffold implantation at 12 weeks post-surgery. (**B** and **C**) Quantification of RUNX2-positive and OCN-positive cells in each group. $^{**}p < 0.01$, $^{***}p < 0.001$ versus the PLGA/n-HA group; $^{\#\#\#}p < 0.001$ versus the PLGA/n-HA/VAN group.

detection and counting of the bacterial load on the scaffold surface and in the adjacent bone of scaffolds. As observed in Figure 9A, the number of bacteria in the adjacent bone tissues in the PLGA/n-HA/VAN and PLGA/n-HA/VAN+DOPA/rhBMP-2 groups was markedly lower than in the PLGA/n-HA group. Besides, we discovered that the bacterial loads of the PLGA/n-HA/VAN and PLGA/n-HA/VAN+DOPA/rhBMP-2 scaffolds were prominently decreased compared with the PLGA/n-HA scaffolds. No significant differences were observed between the PLGA/n-HA/VAN and PLGA/n-HA/VAN +DOPA/rhBMP-2 scaffolds (Figure 9B). Taken together, the PLGA/n-HA/VAN and PLGA/n-HA/VAN+DOPA/rhBMP-2 scaffolds exerted potent antibacterial effect in vivo and could prevent bacteria from entering bone tissues.

Assessment of the Safety of the PLGA/n-HA/VAN+DOPA/rhBMP-2 Scaffolds in vivo

Finally, the toxicity of the scaffolds in IBD rabbit models at 12 weeks post-surgery was evaluated. No obvious histopathological changes were observed in H&E staining images of heart, liver and kidney tissues of both normal and experimental rabbits, indicating the safety of the PLGA/n-HA/VAN+DOPA/rhBMP-2 scaffolds (Figure 10A). In addition, the AST, ALT, BUN, and CK levels of IBD rabbits did not change significantly after implantation with the PLGA/n-HA/VAN+DOPA/rhBMP-2 scaffolds compared with those in normal rabbits (Figure 10B–E).

https://doi.org/10.2147/IJN.S514978

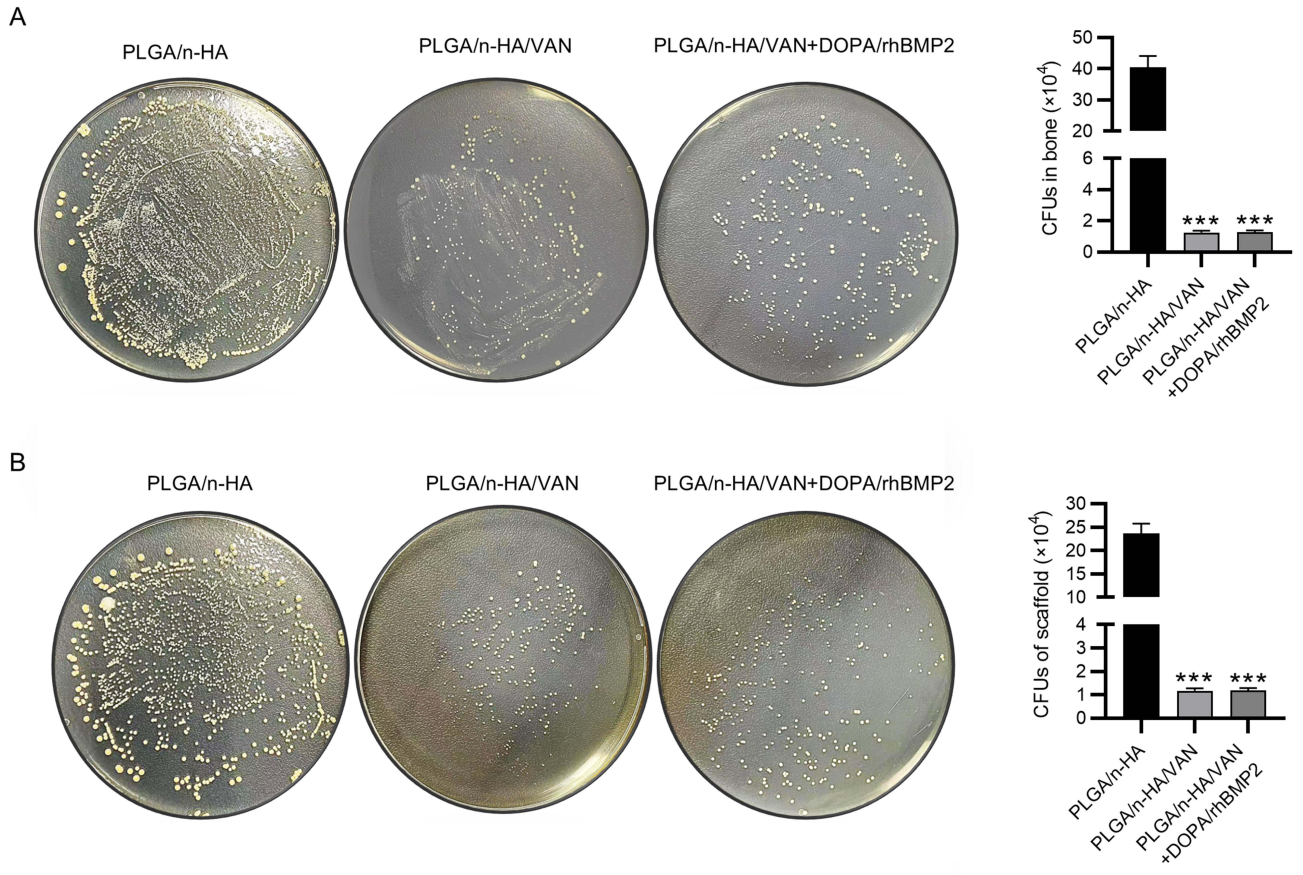

Figure 9 Evaluation of antibacterial properties of scaffolds in vivo. Representative images of viable bacteria and quantification of the CFU counts (**A**) in the adjacent bone of scaffold and (**B**) on the scaffold surface at week 12 post-operatively. ***p < 0.001 versus the PLGA/n-HA group.

Discussion

Repair and reconstruction of bone defects caused by trauma, infection, tumors, surgical debridement for osteomyelitis, and various congenital diseases are important challenges in clinical medicine. The use of autologous or allogeneic grafts is the gold standard for bone defect repair, however, there are many limitations and drawbacks in their clinical application.[57] In the past few decades, bone tissue engineering has emerged as an alternative treatment option and has been developing rapidly. Bionic scaffolds, prepared with various materials, have excellent biological compatibility and can be gradually degraded and absorbed into the human body. They provide a three-dimensional space for cells to live in, just as natural bone does, so that the cells can receive sufficient nutrients to grow in their preformed form on the scaffolds, and ultimately repair the defects.[58] The key to successful early implantation is the rapid osteoblast osteogenic differentiation on the implant without bacterial infection. However, implantation-induced bacterial infection is a serious complication of bone grafting surgery, often leading to worse clinical outcomes, delayed patient recovery, and increased postoperative morbidity.[59] To solve this issue, researchers integrate antibacterial agents with growth factors or osteogenic peptides onto the implant surface.[60] In the present study, we modified 3D-printed PLGA/n-HA scaffolds with antibiotic vancomycin coating, mussel-inspired DOPA grafting, and pro-osteogenic factor BMP-2 immobilization. The schematic diagram illustrating the generation method of our scaffolds is displayed in Figure 11. We discovered that the prepared composite scaffolds PLGA/n-HA/VAN+DOPA/rhBMP-2 exhibited both antibacterial and pro-osteogenic activities in IBD rabbit models.

Polyesters are an important class of synthetic medical polymers with good biocompatibility and biodegradability and are extensively used in various medical applications including surgical sutures, implantable internal fixation devices, and drug slow release.[61] Among polyesters, polylactides are the most well-studied, with polyglycolic acid (PGA), polylactic acid (PLA), polycaprolactone (PCL), and PLA-PGA copolymers (PLGA) cleared by the FDA for bone tissue

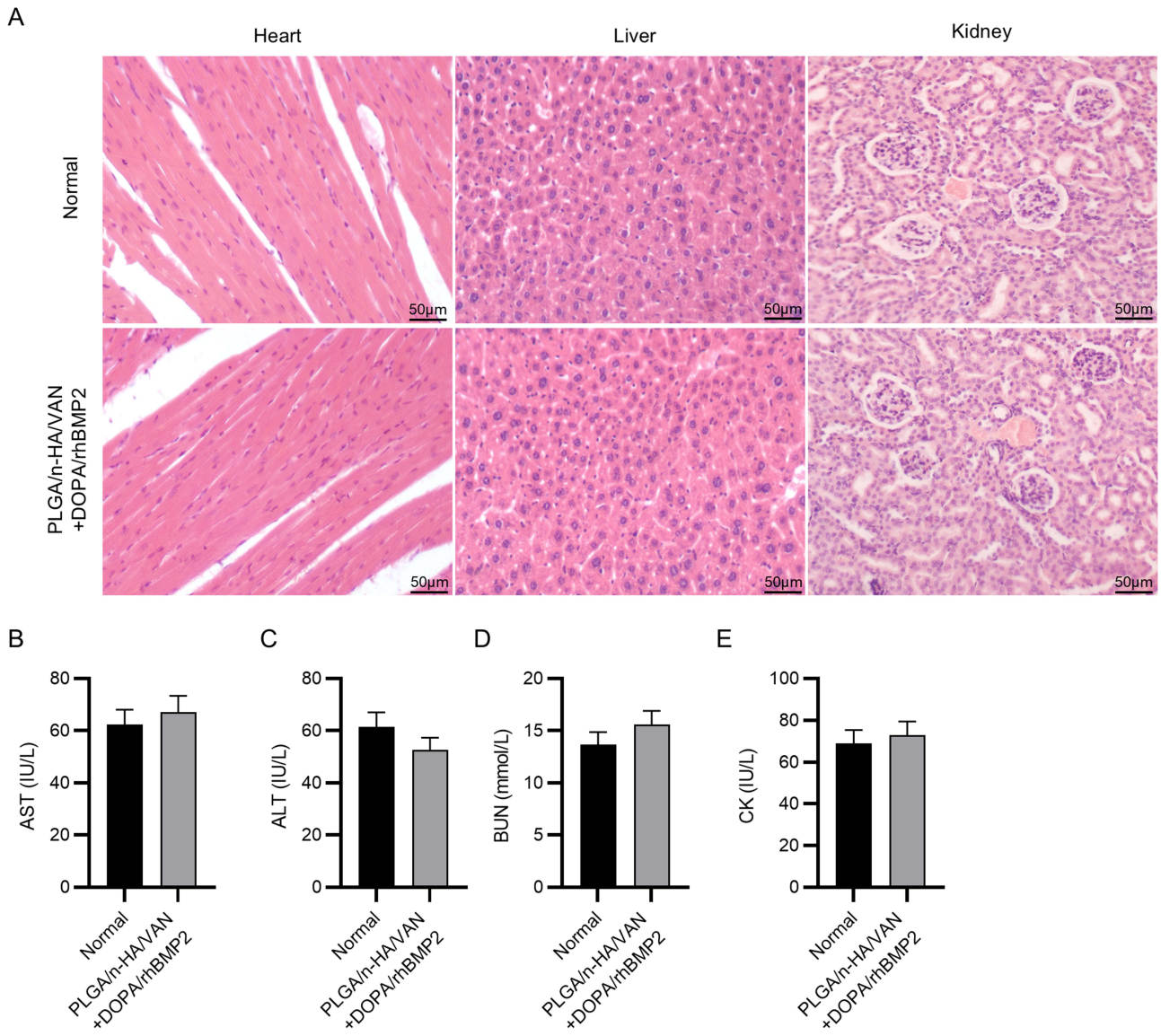

Figure 10 Assessment of the safety of the PLGA/n-HA/VAN+DOPA/rhBMP-2 scaffolds in vivo. (**A**) Representative H&E staining images of heart, liver and kidney tissues of both normal rabbits and scaffold-implanted IBD rabbits at 12 weeks post-surgery. (**B**–**E**) The levels of AST, ALT, BUN, and CK in the serum of rabbits at 12 weeks post-surgery.

engineering. Over the past two decades, a variety of biodegradable synthetic polymer bone grafts have been developed to facilitate regenerative repair of long bone segmental defects, some of which have shown promising results in preclinical animal models.[62] Although synthetic polymers have good mechanical strength, they have the disadvantages of poor hydrophilicity, weak affinity for cells, poor cell adsorption, low osteoconductive potential, uncontrollable degradation rate, high acidity of degradation products, and inflammatory reactions, which make them unsuitable for use in bone tissue engineering alone. Taking into account these inherent shortcomings, synthetic polymers are often compounded with other functional materials such as ceramics to prepare hybrid scaffolds to optimize and improve scaffold performance in bone tissue engineering.[63] Among calcium phosphate ceramics, HA can form chemical bonds with cartilage tissue due to its molecular structure and calcium-phosphorus ratio, which is very similar to the inorganic composition of normal bone, and therefore has excellent bioactivity and osteoinductivity.[64] Increasing studies have demonstrated that the PLGA/HA composite scaffolds effectively promote bone repair and regeneration in experimental animal models with bone defects. For example, Li et al reported that implantation with 3D-printed PLGA/n-HA scaffolds carrying pdgfb-expressing vectors promoted angiogenesis and new bone formation in mouse models of calvarial critical bone defect.[65] Liu et al

https://doi.org/10.2147/IJN.S514978

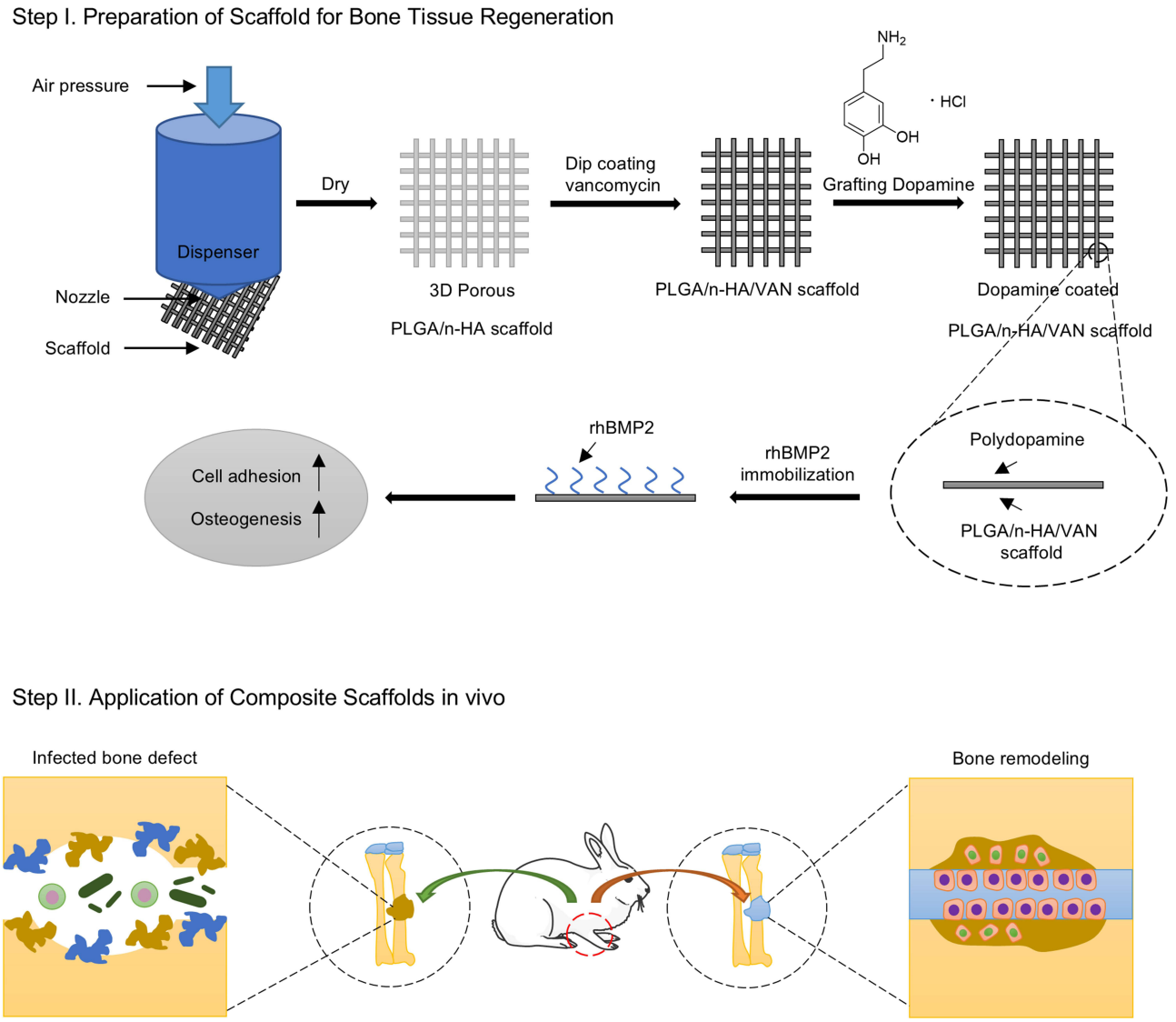

Figure 11 Schematic diagram showing the preparation of the composite scaffolds and implantation of scaffolds into rabbit radial bone defect model.

clarified that composite scaffolds made up of PLGA and Ba/Mg-doped HA significantly improved MC3T3-E1 cell attachment and osteogenic differentiation as well as enhanced the healing of tibial defects and new bone formation in rats.[66] Wei et al suggested that the HA/PLGA composite scaffold containing 45 wt% HA content had six times higher compressive strength than that of the pure PLGA scaffold and displayed the best structure maintenance and osteogenic performance in rabbit femoral defect models.[67]

Bone implant infection is a serious challenge in healthcare. As infectious bacteria accumulate in biofilms and attach to the surface of the device or colonize the surrounding tissues of the implant, the microorganisms can tolerate antibiotics and evade the host defense system.[68] Therefore, it is important to develop bone implants with both osteogenic activity and infection resistance. To address the problem of bone implant infection, people load antibacterial agents like antibiotics, organic bactericides or antibiotics, or inorganic bactericides such as copper/magnesium, silver/strontium, silver/zinc, or titanium dioxide with growth factors or osteogenic peptides on the surface of 3D-printed bone implant scaffolds, endowing the implants with excellent antimicrobial properties.[69,70] Makiishi et al found that implantation of composite granules consisting of HA and gatifloxacine-loaded PLGA in bone defects formed after osteomyelitis lesion debridement in the rabbit mandible alleviated inflammation, controlled bacterial infection, and induced new bone formation.[71] We previously revealed that linezolid-loaded 3D-printed PLGA/n-HA scaffolds better attenuated bone

infection and promoted bone healing in rabbit radius defect models than PLGA and PLGA/n-HA scaffolds.[72] Chen et al used the DIW printing technique to homogeneously mix PLGA with silver nanoparticles (AgNPs) to fabricate antibacterial scaffolds, which showed potent antibacterial effects against *Escherichia coli* and *Staphylococcus aureus* and exhibited good cellular compatibility to enhance MC3T3-E1 cell survival and proliferation.[73] Feng et al clarified that the poly-L-lactic acid (PLLA) scaffolds exhibited enhanced mechanical properties, good biocompatibility, and effective antibacterial properties against *Staphylococcus aureus* and *Escherichia coli* due to the addition of the titanium dioxide/reduced graphene oxide (TiO_2/rGO) composites.[74] Vancomycin is a glycopeptide antibacterial drug with a triple bactericidal mechanism, which kills bacteria by inhibiting the synthesis of the bacterial cell wall, altering the permeability of the bacterial cell membrane, and blocking the synthesis of bacterial intracytoplasmic RNA, and is widely used in the treatment of various gram-positive bacterial infections.[75] Considering that intravenous vancomycin has adverse systemic effects, such as allergic reactions, hypotension, and nephrotoxicity, local release of vancomycin can produce sufficient concentrations on site to avoid the above side effects.[76] Previous studies have elucidated the antibacterial effects of vancomycin-loaded scaffolds as effective bone grafting materials. For example, Li et al confirmed that the PLA/n-HA composite scaffolds loaded with vancomycin/PLGA sustained release microspheres not only inhibited the growth of *Staphylococcus aureus* and resisted local infection, but also facilitated bone regeneration in rabbits with femur infective defect.[77] Chen et al constructed a vancomycin-loaded nanodiamond-type 45S5 bioactive glass composite scaffold and confirmed its excellent biocompatibility, antibacterial, and osteogenic activities in rabbit bone marrow mesenchymal stem cells and in IBD rabbit models.[29] Cao et al disclosed that bone infection induced by *Staphylococcus aureus* and methicillin-resistant *S. aureus* (MRSA) was alleviated in rabbit models of chronic osteomyelitis after implantation with vancomycin-loaded bone-like HA/poly amino acid scaffolds.[78] In our study, we found that the cumulative vancomycin-elution rate in the vancomycin-loaded PLGA/n-HA/VAN and PLGA/n-HA/VAN+DOPA/rhBMP-2 composite scaffolds in vitro gradually increased as time passed on, and reached close to 90% at day 30. Additionally, in vivo results showed that the bacterial load on the scaffold surface and in the bone tissues adjacent to the scaffolds was prominently lower in the PLGA/n-HA/VAN and PLGA/n-HA/VAN+DOPA/rhBMP-2 groups than in the PLGA/n-HA group. However, the bacteria in the PLGA/n-HA group survived adequately and had already entered the bone tissue, suggesting that the PLGA/n-HA scaffold had no effect on the bacteria. Therefore, vancomycin-loaded PLGA/n-HA scaffolds had a more significant antibacterial effect in IBD rabbit models than unloaded PLGA/n-HA scaffolds.

The wettability of the implant material surface is an important factor affecting the biocompatibility and osseointegration ability of the implant material.[79] It has been confirmed that surface wettability is a vital factor contributing to the adhesion of osteoblasts on biomaterials, which is pivotal for bone tissue regeneration.[80] PLGA is a hydrophobic polymer without active sites for cellular attachment, which hinders cell adhesion and migration. Although several methods including gas forming and particulate leaching (GF/PL), phase separation, solvent casting and particulate leaching (SC/PL), and ceramic coating by simulated body fluid (SBF) have been explored to develop biodegradable polymer/ceramic composite scaffolds, these methods are time-consuming and refer to the use of cytotoxic organic solvents.[81] Moreover, PLGA solution can curb the exposure of bioactive ceramics on the scaffold surface and decrease the contact between ceramics and osteoblast in the composite scaffolds.[82] Gland cells containing secretory granules have been discovered in the foot of the mussel Mytilus edulis, which can secret adhesion proteins that have super strong adhesion properties and can be tightly adhered to the surface of various substrates. These adhesion proteins are rich in amino acids with catechol groups, namely L-3,4-dihydroxyphenylalanine (L-DOPA), a precursor of dopamine, which is a key factor for the superb adhesion of these proteins.[83] Dopamine can be hydrogen bonded, ligand bonded and covalently bonded with a variety of substrates, and thus also has excellent adhesion properties. Under alkaline conditions, dopamine spontaneously oxidizes and self-polymerizes to form DOPA, which can be used to modify the properties of almost any material surface, such as enhancing the wettability and adhesion of the material.[84] The DOPA coating technique has been applied in a wide range of fields including surface functionalization of liposomes, modification of graphene oxide/superhydrophobic surface, carbon nanotube functionalization, antibacterial surface, DOPA capsule fabrication and assembly for drug delivery, water detoxification, corrosion protection, biomineralization, and microfluidics.[85–87] Besides, the internal surfaces in complicated and porous 3D materials can be functionalized by the dip-coating of

DOPA. The DOPA coating is a crucial method that converts the hydrophobic and non-adhesive surface of the 3D polymer scaffolds into the hydrophilic and cell-adhesive one without destroying the polymer substrate.[88] Previously, Jo et al revealed that DOPA coating combined with HA immobilization significantly enhanced the hydrophilicity of the 3D-printed PCL scaffolds, which had good cell infiltration and was conducive to cell proliferation and migration.[85] Yang et al reported that implantation with HA- and DOPA-coated PGA scaffolds in critical-sized skull defects in mice resulted in far more extensive bone regeneration than implantation with PGA, DOPA-coated PGA, or HA-coated PGA scaffolds.[81] In our study, to increase the bone like-cell attachment and facilitate cellular migration, we changed the wettability of the PLGA/n-HA scaffolds from hydrophobic to superhydrophilic by coating the scaffolds using DOPA chemistry. As mentioned earlier, the amine and catechol groups in DOPA enable the formation of polymer on any substrate with weak alkaline, which gives it great potential for bone regeneration.[89] Therefore, increasing studies have focused on combining DOPA with BMPs, and BMPs can be covalently bound to 3D-printed polymer scaffolds using DOPA chemistry to achieve the effective delivery of BMPs with a sustained release pattern, thereby promoting bone tissue regeneration.[90]

Bone tissue engineering and regenerative medicine make it possible to reconstruct bone defects by loading growth factors onto the scaffold material.[91] The BMP family, which is composed of multifunctional cytokines belonging to the TGF-β superfamily of proteins, is well known to regulate cell differentiation and proliferation and facilitate osteogenesis.[92] Among the BMP family, BMP-2 has been validated as a critical osteoinductive growth factor that induces bone formation through stimulating the osteogenic differentiation of mesenchymal stem cells and enhancing the recruitment and angiogenesis of osteoblast progenitor cells.[93] The clinical use of recombinant BMP-2 in maxillary sinus reconstructive surgery, tibial shaft repair, and spinal fusion surgery has been approved by the FDA.[94] Nevertheless, there exist disadvantages to the direct incorporation of growth factors into the scaffolds, including uncontrollable burst release and low loading capacity.[95] Therefore, controlled sustained release of BMP-2 must be achieved by an ideal carrier to promote the long-term activity of BMP-2 in specific environments for efficient bone regeneration. DOPA coating can ensure good bonding with the scaffold and at the same time, it can realize the slow release of the loaded drug and effectively avoid the burst release phenomenon.[96] Previously, Lee et al fabricated 3D-printed PCL scaffolds with rhBMP-2 grafting through DOPA chemistry, which considerably promoted MC3T3-E1 cell proliferation and osteogenesis differentiation in vitro compared with PCL scaffolds and DOPA-coated scaffolds.[51] Ko et al utilized DOPA chemistry to facilitate the immobilization of BMP-2 peptide on PLGA scaffolds, and the modified scaffolds exhibited better effects on enhancing human adipose-derived stem cell osteogenic differentiation and calcium mineralization in vitro as well as promoting bone formation in animal models of critical-sized calvarial bone defects than bare scaffolds.[97] Moreover, Cho et al prepared BMP-2 immobilized poly(l-lactide) (PLLA) nanofibers through DOPA coating, whose implantation into the critical-sized cranium defects in mice effectively facilitated bone formation in vivo.[89] In our research, BMP-2 was continuously released from the PLGA/n-HA/VAN+DOPA/rhBMP-2 scaffolds over a long time, with almost complete release by day 25, suggesting that the PLGA/n-HA/VAN+DOPA/rhBMP-2 composite scaffolds achieved sustained release of BMP-2 through DOPA coating technology.

Before evaluating the osteogenesis activity of the composite scaffolds in vitro, we confirmed the biocompatibility, the basis of implantable materials, through live/dead cell staining and CCK-8 assay. The data showed that incubation with the PLGA/n-HA/VAN+DOPA/rhBMP-2 scaffolds promoted MC3T3-E1 cell survival and proliferation compared with the PLGA/n-HA and PLGA/n-HA/VAN scaffolds, which indicated that DOPA/rhBMP-2 coating remarkably improved the biocompatibility of the PLGA/n-HA scaffolds. ALP is one of the phenotypic markers of osteoblasts, which can directly reflect the activity or function of osteoblasts.[98] In addition, the formation of calcium nodules is unique to osteoblasts, and calcium deposits are evidence of new bone formation.[99] The enhancement in the ALP activity and calcium deposition observed in ALP and ARS staining demonstrated that the PLGA/n-HA/VAN+DOPA/rhBMP-2 scaffolds have well-established osteogenesis. Given that implant fixation or prosthetic device manipulation is difficult in smaller rodents, such as rats and mice, we created segmental bone defects in rabbit radius with reference to previous studies.[100,101] Three scaffolds were contaminated with the prepared Staphylococcus aureus and then respectively implanted into the defect site in rabbit middle radius. At 12 weeks after the surgery, micro-CT analysis was performed to observe new bone formation. Obvious osteomyelitis and irregular bone formation without bone healing were observed at the defect site in both PLGA/n-HA and

PLGA/n-HA/VAN groups, while the growth of new bones into the scaffold and formation of continuous healing bones at the defect area without any infection signs were discovered in the PLGA/n-HA/VAN+DOPA/rhBMP-2 group. The increment in BV/TV ratio after PLGA/n-HA/VAN+DOPA/rhBMP-2 scaffold implantation also validated the promotion of this composite scaffold on new bone formation and bone healing. The subsequent histopathological staining of bone tissues surrounding the scaffolds revealed that implantation with the PLGA/n-HA/VAN+DOPA/rhBMP-2 scaffolds evidently decreased the aggregation of pus cells, promoted the formation of a large number of new bones, and enhanced the integrity, regularity, and density of bone trabeculae compared with the other two scaffolds. OCN is a non-collagenous protein secreted and synthesized primarily by osteoblasts, which promotes bone formation and mineralization by participating in the deposition of calcium and phosphorus.[102] RUNX2 is an osteogenic differentiation-specific transcription factor that regulates the transcription of many genes related to osteogenic differentiations, and its expression and activity have a decisive influence on bone formation and maintenance.[103] In our study, we discovered that the PLGA/n-HA scaffolds grafted with vancomycin/DOPA/rhBMP-2 strikingly upregulated OCN and RUNX2 expression in radius tissues of IBD rabbit models, which indicated that the beneficial role of this composite scaffold in new bone formation was dependent on its regulation on osteogenic genes.

Limitations

To be honest, although our preliminary results are successful, this study has several limitations. First, the significant differences observed in our experiments were limited to a small size of animals in each group. Second, in addition to the most common *Staphylococcus aureus*, the pathogenic bacteria of IBD also include *Enterococcus spp., Pseudomonas aeruginosa, Escherichia coli*, and *Cutibacterium acnes*. Our study only used *Staphylococcus aureus* to induce experimental IBD in rabbit models. Whether the composite scaffold exerts antibacterial effects on other pathogens that induce IBD requires further exploration. Third, existing 3D printing technologies are often based on photocuring technology to trigger photopolymerization in transparent inks, which limits material selection and build size. The recent emergence of new technologies ultrasonic 3D printing technology, especially deep-penetration acoustic volume printing (DAVP) technology, using viscoelastic ink and high-intensity focused ultrasound for 3D printing, not only achieves the characteristics of large printing depth, rapid sonothermal polymerization, and low acoustic streaming but also allows printing at centimeter depths through biological tissues.[104] It holds great promise in biomedical applications and is expected to be widely used in the field of bone regeneration. In future studies, ultrasound systems can be used for the 3D printing of vancomycin/DOPA/rhBMP-2-coated PLGA/n-HA scaffolds and whether the obtained scaffold has better antibacterial and osteoinductive activities in IBD should be explored. Finally, the efficacy of clinical translation of the results of this study is still unknown. The translation of this scaffold technology to clinical use is faced with several challenges, one of which is that the diverse structural architectures and biomechanical properties of different regions of human tissues and the complex microenvironment increase the difficulty of bionic printing. Therefore, future studies need to focus on acquiring precise data to print personalized scaffolds to improve their osseointegration ability.

Conclusions

Collectively, our study confirmed that the PLGA/n-HA scaffolds grafted with vancomycin/DOPA/rhBMP-2 exhibited better efficacy in promoting proliferation and osteogenic differentiation of MC3T3-E1 cells in vitro as well as facilitating bone regeneration and suppressing bone infection in IBD rabbit models than the PLGA/n-HA scaffolds without any coating or with only vancomycin coating. Accordingly, this novel composite scaffold bearing both antibacterial and pro-osteogenic activities has therapeutic potential for IBD.

Data Sharing Statement

The datasets used or analyzed during the current study are available from the corresponding author on reasonable request.

Ethical Approval

All experiments were approved by the Animal Ethics Committee of First People's Hospital of Kashgar.

Acknowledgment

The authors appreciate all the participants providing supports for this study.

Author Contributions

All authors made a significant contribution to the work reported, whether that is in the conception, study design, execution, acquisition of data, analysis and interpretation, or in all these areas; took part in drafting, revising or critically reviewing the article; gave final approval of the version to be published; have agreed on the journal to which the article has been submitted; and agree to be accountable for all aspects of the work.

Funding

The work was supported by Tianshan Talents Program (No.2022TSYCJC0009).

Disclosure

The authors declare that they have no competing interests.

References

1. Li X, Huang X, Li L, et al. LL-37-Coupled Porous Composite Scaffold for the Treatment of Infected Segmental Bone Defect. *Pharmaceutics*. 2022;15(1):88. doi:10.3390/pharmaceutics15010088
2. Okike K, Bhattacharyya T. Trends in the management of open fractures. A critical analysis. *J Bone Joint Surg Am*. 2006;88(12):2739–2748. doi:10.2106/00004623-200612000-00025
3. Wang M, Li H, Yang Y, et al. A 3D-bioprinted scaffold with doxycycline-controlled BMP2-expressing cells for inducing bone regeneration and inhibiting bacterial infection. *Bioact Mater*. 2021;6(5):1318–1329. doi:10.1016/j.bioactmat.2020.10.022
4. Qian H, Lei T, Hua L, et al. Fabrication, bacteriostasis and osteointegration properties researches of the additively-manufactured porous tantalum scaffolds loading vancomycin. *Bioact Mater*. 2023;24:450–462. doi:10.1016/j.bioactmat.2022.12.013
5. Lu H, Liu Y, Guo J, et al. Biomaterials with antibacterial and osteoinductive properties to repair infected bone defects. *Int J Mol Sci*. 2016;17(3):334. doi:10.3390/ijms17030334
6. Keller L, Regiel-Futyra A, Gimeno M, et al. Chitosan-based nanocomposites for the repair of bone defects. *Nanomedicine*. 2017;13(7):2231–2240. doi:10.1016/j.nano.2017.06.007
7. Feng P, et al. Structural and functional adaptive artificial bone: materials, fabrications, and properties. *Adv Funct Mater* 2023;33(23):2214726.
8. Feng P, Liu L, Yang F, et al. Shape/properties collaborative intelligent manufacturing of artificial bone scaffold: structural design and additive manufacturing process. *Biofabrication*. 2025;17(1):012005. doi:10.1088/1758-5090/ad905f
9. Damiri F, Fatimi A, Liu Y, et al. Recent advances in 3D bioprinted polysaccharide hydrogels for biomedical applications: a comprehensive review. *Carbohydr Polym*. 2025;348(Pt B):122845. doi:10.1016/j.carbpol.2024.122845
10. Zhang L, Yang G, Johnson BN, et al. Three-dimensional (3D) printed scaffold and material selection for bone repair. *Acta Biomater*. 2019;84:16–33. doi:10.1016/j.actbio.2018.11.039
11. Sugiaman VK, Naliani S, Pranata N, et al. Polymeric scaffolds used in dental pulp regeneration by tissue engineering approach. *Polymers*. 2023;15(5):1082. doi:10.3390/polym15051082
12. Bharadwaz A, Jayasuriya AC. Recent trends in the application of widely used natural and synthetic polymer nanocomposites in bone tissue regeneration. *Mater Sci Eng C Mater Biol Appl*. 2020;110:110698. doi:10.1016/j.msec.2020.110698
13. Guo B, Ma PX. Conducting polymers for tissue engineering. *Biomacromolecules*. 2018;19(6):1764–1782. doi:10.1021/acs.biomac.8b00276
14. Rocha CV, Gonçalves V, da Silva MC, et al. PLGA-based composites for various biomedical applications. *Int J Mol Sci*. 2022;23(4):2034. doi:10.3390/ijms23042034
15. Bhuiyan DB, Middleton JC, Tannenbaum R, et al. Mechanical properties and osteogenic potential of hydroxyapatite-PLGA-collagen biomaterial for bone regeneration. *J Biomater Sci Polym Ed*. 2016;27(11):1139–1154. doi:10.1080/09205063.2016.1184121
16. Pan Z, Ding J. Poly(lactide-co-glycolide) porous scaffolds for tissue engineering and regenerative medicine. *Interface Focus*. 2012;2(3):366–377. doi:10.1098/rsfs.2011.0123
17. Damiri F, Fatimi A, Magdalena Musuc A, et al. Nano-hydroxyapatite (nHAp) scaffolds for bone regeneration: preparation, characterization and biological applications. *J Drug Deliv Sci Technol*. 2024;95:105601. doi:10.1016/j.jddst.2024.105601
18. Qian J, Xu W, Yong X, et al. Fabrication and in vitro biocompatibility of biomorphic PLGA/nHA composite scaffolds for bone tissue engineering. *Mater Sci Eng C Mater Biol Appl*. 2014;36:95–101. doi:10.1016/j.msec.2013.11.047
19. Shuai C, Yang W, Feng P, et al. Accelerated degradation of HAP/PLLA bone scaffold by PGA blending facilitates bioactivity and osteoconductivity. *Bioact Mater*. 2021;6(2):490–502. doi:10.1016/j.bioactmat.2020.09.001
20. Jose MV, Thomas V, Xu Y, et al. Aligned bioactive multi-component nanofibrous nanocomposite scaffolds for bone tissue engineering. *Macromol Biosci*. 2010;10(4):433–444. doi:10.1002/mabi.200900287
21. Kim SS, Sun Park M, Jeon O, et al. Poly(lactide-co-glycolide)/hydroxyapatite composite scaffolds for bone tissue engineering. *Biomaterials*. 2006;27(8):1399–1409. doi:10.1016/j.biomaterials.2005.08.016
22. Yang Y, Yang S, Wang Y, et al. Anti-infective efficacy, cytocompatibility and biocompatibility of a 3D-printed osteoconductive composite scaffold functionalized with quaternized chitosan. *Acta Biomater*. 2016;46:112–128. doi:10.1016/j.actbio.2016.09.035

23. Johnson CT, García AJ. Scaffold-based anti-infection strategies in bone repair. *Ann Biomed Eng*. 2015;43(3):515–528. doi:10.1007/s10439-014-1205-3
24. Masters EA, Ricciardi BF, Bentley KLDM, et al. Skeletal infections: microbial pathogenesis, immunity and clinical management. *Nat Rev Microbiol*. 2022;20(7):385–400. doi:10.1038/s41579-022-00686-0
25. Chen ZY, Gao S, Zhang Y-W, et al. Antibacterial biomaterials in bone tissue engineering. *J Mater Chem B*. 2021;9(11):2594–2612. doi:10.1039/D0TB02983A
26. Ford CA, Cassat JE. Advances in the local and targeted delivery of anti-infective agents for management of osteomyelitis. *Expert Rev Anti Infect Ther*. 2017;15(9):851–860. doi:10.1080/14787210.2017.1372192
27. Mo X, Zhang D, Liu K, et al. Nano-hydroxyapatite composite scaffolds loaded with bioactive factors and drugs for bone tissue engineering. *Int J Mol Sci*. 2023;24(2):1291. doi:10.3390/ijms24021291
28. Gardete S, Tomasz A. Mechanisms of vancomycin resistance in Staphylococcus aureus. *J Clin Invest*. 2014;124(7):2836–2840. doi:10.1172/JCI68834
29. Chen M, Li Y, Hou W-X, et al. The antibacterial effect, biocompatibility, and osteogenesis of vancomycin-nanodiamond composite scaffold for infected bone defects. *Int J Nanomed*. 2023;18:1365–1380. doi:10.2147/IJN.S397316
30. Bruniera FR, Ferreira FM, Saviolli LRM, et al. The use of vancomycin with its therapeutic and adverse effects: a review. *Eur Rev Med Pharmacol Sci*. 2015;19(4):694–700.
31. Han W, Zhang L, Yu L-J, et al. Effect of local delivery of vancomycin and tobramycin on bone regeneration. *Orthop Surg*. 2021;13(5):1654–1661. doi:10.1111/os.13020
32. Iglesias-Mejuto A, Magariños B, Ferreira-Gonçalves T, et al. Vancomycin-loaded methylcellulose aerogel scaffolds for advanced bone tissue engineering. *Carbohydr Polym*. 2024;324:121536. doi:10.1016/j.carbpol.2023.121536
33. El Bialy I, Jiskoot W, Reza Nejadnik M. Formulation, delivery and stability of bone morphogenetic proteins for effective bone regeneration. *Pharm Res*. 2017;34(6):1152–1170. doi:10.1007/s11095-017-2147-x
34. Wu M, Chen G, Li YP. TGF-β and BMP signaling in osteoblast, skeletal development, and bone formation, homeostasis and disease. *Bone Res*. 2016;4:16009. doi:10.1038/boneres.2016.9
35. Zhang X, Li J, Chen J, et al. Enhanced bone regeneration via PHA scaffolds coated with polydopamine-captured BMP2. *J Mater Chem B*. 2022;10(32):6214–6227. doi:10.1039/D2TB01122K
36. Shweikeh F, Hanna G, Bloom L, et al. Assessment of outcome following the use of recombinant human bone morphogenetic protein-2 for spinal fusion in the elderly population. *J Neurosurg Sci*. 2016;60(2):256–271.
37. Gillman CE, Jayasuriya AC. FDA-approved bone grafts and bone graft substitute devices in bone regeneration. *Mater Sci Eng C Mater Biol Appl*. 2021;130:112466. doi:10.1016/j.msec.2021.112466
38. Loozen LD, Kruyt MC, Kragten AHM, et al. BMP-2 gene delivery in cell-loaded and cell-free constructs for bone regeneration. *PLoS One*. 2019;14(7):e0220028. doi:10.1371/journal.pone.0220028
39. Xu T, Sheng L, He L, et al. Enhanced osteogenesis of hydroxyapatite scaffolds by coating with BMP-2-loaded short polylactide nanofiber: a new drug loading method for porous scaffolds. *Regen Biomater*. 2020;7(1):91–98. doi:10.1093/rb/rbz040
40. Jarrar H, Çetin Altındal D, Gümüşderelioğlu M. Effect of melatonin/BMP-2 co-delivery scaffolds on the osteoclast activity. *J Mater Sci Mater Med*. 2021;32(4):32. doi:10.1007/s10856-021-06502-0
41. Ma R, Su Y, Cao R, et al. Enhanced osteogenic activity and bone repair ability of PLGA/MBG scaffolds doped with ZIF-8 nanoparticles loaded with BMP-2. *Int J Nanomed*. 2023;18:5055–5072. doi:10.2147/IJN.S423985
42. Haidar ZS, Hamdy RC, Tabrizian M. Delivery of recombinant bone morphogenetic proteins for bone regeneration and repair. Part B: delivery systems for BMPs in orthopaedic and craniofacial tissue engineering. *Biotechnol Lett*. 2009;31(12):1825–1835. doi:10.1007/s10529-009-0100-8
43. Liu Y, Huse RO, de Groot K, et al. Delivery mode and efficacy of BMP-2 in association with implants. *J Dent Res*. 2007;86(1):84–89. doi:10.1177/154405910708600114
44. Damiri F, Fatimi A, Santos ACP, et al. Smart stimuli-responsive polysaccharide nanohydrogels for drug delivery: a review. *J Mater Chem B*. 2023;11(44):10538–10565. doi:10.1039/D3TB01712E
45. Zhou Y, Yang Y, Liu R, et al. Research progress of polydopamine hydrogel in the prevention and treatment of oral diseases. *Int J Nanomed*. 2023;18:2623–2645. doi:10.2147/IJN.S407044
46. Chen Z, Zhang Z, Feng J, et al. Influence of mussel-derived bioactive BMP-2-decorated PLA on MSC behavior in vitro and verification with osteogenicity at ectopic sites in vivo. *ACS Appl Mater Interfaces*. 2018;10(14):11961–11971. doi:10.1021/acsami.8b01547
47. Chen Z, Li Q, Chen J, et al. Immobilization of serum albumin and peptide aptamer for EPC on polydopamine coated titanium surface for enhanced in-situ self-endothelialization. *Mater Sci Eng C Mater Biol Appl*. 2016;60:219–229. doi:10.1016/j.msec.2015.11.044
48. Lee H, Dellatore SM, Miller WM, et al. Mussel-inspired surface chemistry for multifunctional coatings. *Science*. 2007;318(5849):426–430. doi:10.1126/science.1147241
49. Zhu M, Li K, Zhu Y, et al. 3D-printed hierarchical scaffold for localized isoniazid/rifampin drug delivery and osteoarticular tuberculosis therapy. *Acta Biomater*. 2015;16:145–155. doi:10.1016/j.actbio.2015.01.034
50. Pérez-Davila S, Potel-Alvarellos C, Carballo R, et al. Vancomycin-loaded 3D-printed polylactic acid-hydroxyapatite scaffolds for bone tissue engineering. *Polymers*. 2023;15(21):4250. doi:10.3390/polym15214250
51. Lee SJ, Lee D, Yoon TR, et al. Surface modification of 3D-printed porous scaffolds via mussel-inspired polydopamine and effective immobilization of rhBMP-2 to promote osteogenic differentiation for bone tissue engineering. *Acta Biomater*. 2016;40:182–191. doi:10.1016/j.actbio.2016.02.006
52. Qiao Z, Zhang W, Jiang H, et al. 3D-printed composite scaffold with anti-infection and osteogenesis potential against infected bone defects. *RSC Adv*. 2022;12(18):11008–11020. doi:10.1039/D2RA00214K
53. Yang Y, Chu L, Yang S, et al. Dual-functional 3D-printed composite scaffold for inhibiting bacterial infection and promoting bone regeneration in infected bone defect models. *Acta Biomater*. 2018;79:265–275. doi:10.1016/j.actbio.2018.08.015
54. Lucke M, Schmidmaier G, Sadoni S, et al. A new model of implant-related osteomyelitis in rats. *J Biomed Mater Res B Appl Biomater*. 2003;67B(1):593–602. doi:10.1002/jbm.b.10051

55. Lee H, Rho J, Messersmith PB. Facile conjugation of biomolecules onto surfaces via mussel adhesive protein inspired coatings. *Adv Mater*. 2009;21(4):431–434. doi:10.1002/adma.200801222
56. Burgers TA, Mason J, Niebur G, et al. Compressive properties of trabecular bone in the distal femur. *J Biomech*. 2008;41(5):1077–1085. doi:10.1016/j.jbiomech.2007.11.018
57. Agarwal R, García AJ. Biomaterial strategies for engineering implants for enhanced osseointegration and bone repair. *Adv Drug Deliv Rev*. 2015;94:53–62. doi:10.1016/j.addr.2015.03.013
58. Zhou S, Liu S, Wang Y, et al. Advances in the study of bionic mineralized collagen, PLGA, magnesium ionomer materials, and their composite scaffolds for bone defect treatment. *J Funct Biomater*. 2023;14(8):406. doi:10.3390/jfb14080406
59. Gorzelanny C, Kmeth R, Obermeier A, et al. Silver nanoparticle-enriched diamond-like carbon implant modification as a mammalian cell compatible surface with antimicrobial properties. *Sci Rep*. 2016;6:22849. doi:10.1038/srep22849
60. Hasani-Sadrabadi MM, Pouraghaei S, Zahedi E, et al. Antibacterial and osteoinductive implant surface using layer-by-layer assembly. *J Dent Res*. 2021;100(10):1161–1168. doi:10.1177/00220345211029185
61. Zamboulis A, Nakiou EA, Christodoulou E, et al. Polyglycerol hyperbranched polyesters: synthesis, properties and pharmaceutical and biomedical applications. *Int J Mol Sci*. 2019;20(24):6210. doi:10.3390/ijms20246210
62. Alonso-Fernández I, Haugen HJ, López-Peña M, et al. Use of 3D-printed polylactic acid/bioceramic composite scaffolds for bone tissue engineering in preclinical in vivo studies: a systematic review. *Acta Biomater*. 2023;168:1–21. doi:10.1016/j.actbio.2023.07.013
63. Alizadeh-Osgouei M, Li Y, Wen C. A comprehensive review of biodegradable synthetic polymer-ceramic composites and their manufacture for biomedical applications. *Bioact Mater*. 2019;4(1):22–36. doi:10.1016/j.bioactmat.2018.11.003
64. Ielo I, Calabrese G, De Luca G, et al. Recent advances in hydroxyapatite-based biocomposites for bone tissue regeneration in orthopedics. *Int J Mol Sci*. 2022;23(17):9721. doi:10.3390/ijms23179721
65. Li J, Xu Q, Teng B, et al. Investigation of angiogenesis in bioactive 3-dimensional poly(d,l-lactide-co-glycolide)/nano-hydroxyapatite scaffolds by in vivo multiphoton microscopy in murine calvarial critical bone defect. *Acta Biomater*. 2016;42:389–399. doi:10.1016/j.actbio.2016.06.024
66. Liu X, Ma Y, Chen M, et al. Ba/Mg co-doped hydroxyapatite/PLGA composites enhance X-ray imaging and bone defect regeneration. *J Mater Chem B*. 2021;9(33):6691–6702. doi:10.1039/D1TB01080H
67. Wei J, Yan Y, Gao J, et al. 3D-printed hydroxyapatite microspheres reinforced PLGA scaffolds for bone regeneration. *Biomater Adv*. 2022;133:112618. doi:10.1016/j.msec.2021.112618
68. Giavaresi G, Bertazzoni Minelli E, Sartori M, et al. Microbiological and pharmacological tests on new antibiotic-loaded PMMA-based composites for the treatment of osteomyelitis. *J Orthop Res*. 2012;30(3):348–355. doi:10.1002/jor.21531
69. Inzana JA, Trombetta RP, Schwarz EM, et al. 3D printed bioceramics for dual antibiotic delivery to treat implant-associated bone infection. *Eur Cell Mater*. 2015;30:232–247. doi:10.22203/eCM.v030a16
70. Zhang Y, Zhai D, Xu M, et al. 3D-printed bioceramic scaffolds with antibacterial and osteogenic activity. *Biofabrication*. 2017;9(2):025037. doi:10.1088/1758-5090/aa6ed6
71. Makiishi J, Matsuno T, Ito A, et al. In vitro/in vivo evaluation of the efficacy of gatifloxacine-loaded PLGA and hydroxyapatite composite for treating osteomyelitis. *Dent Mater J*. 2017;36(6):714–723. doi:10.4012/dmj.2016-338
72. Ke Re Mu ALM, Liang ZL, Chen L, et al. 3D printed PLGA scaffold with nano-hydroxyapatite carrying linezolid for treatment of infected bone defects. *Biomed Pharmacother*. 2024;172:116228. doi:10.1016/j.biopha.2024.116228
73. Chen F, Han J, Guo Z, et al. Antibacterial 3D-printed silver nanoparticle/poly lactic-co-glycolic acid (PLGA) scaffolds for bone tissue engineering. *Materials*. 2023;16(11):3895.
74. Feng P, Tian H, Yang F, et al. Reduced graphene oxide-mediated electron-hole separation using titanium dioxide increases the photocatalytic antibacterial activity of bone scaffolds. *Bio-Des Manuf*. 2025;8(1):100–115. doi:10.1631/bdm.2300372
75. Álvarez R, López Cortés LE, Molina J, et al. Optimizing the clinical use of vancomycin. *Antimicrob Agents Chemother*. 2016;60(5):2601–2609. doi:10.1128/AAC.03147-14
76. Alegrete N, Sousa SR, Padrão T, et al. Vancomycin-loaded, nanohydroxyapatite-based scaffold for osteomyelitis treatment: in vivo rabbit toxicological tests and in vivo efficacy tests in a sheep model. *Bioengineering*. 2023;10(2):206. doi:10.3390/bioengineering10020206
77. Li J, Li K, Du Y, et al. Dual-nozzle 3D printed nano-hydroxyapatite scaffold loaded with vancomycin sustained-release microspheres for enhancing bone regeneration. *Int J Nanomed*. 2023;18:307–322. doi:10.2147/IJN.S394366
78. Cao Z, Jiang D, Yan L, et al. In vitro and in vivo drug release and antibacterial properties of the novel vancomycin-loaded bone-like hydroxyapatite/poly amino acid scaffold. *Int J Nanomed*. 2017;12:1841–1851. doi:10.2147/IJN.S122864
79. Miron RJ, Bohner M, Zhang Y, et al. Osteoinduction and osteoimmunology: emerging concepts. *Periodontol*. 2024;94(1):9–26. doi:10.1111/prd.12519
80. Boyan BD, Lotz EM, Schwartz Z. (*) roughness and hydrophilicity as osteogenic biomimetic surface properties. *Tissue Eng Part A*. 2017;23(23–24):1479–1489. doi:10.1089/ten.tea.2017.0048
81. Yang HS, Park J, La WG, et al. 3,4-dihydroxyphenylalanine-assisted hydroxyapatite nanoparticle coating on polymer scaffolds for efficient osteoconduction. *Tissue Eng Part C Methods*. 2012;18(4):245–251. doi:10.1089/ten.tec.2011.0373
82. Kim SS, Ahn K-M, Park MS, et al. A poly(lactide- co -glycolide)/hydroxyapatite composite scaffold with enhanced osteoconductivity. *J Biomed Mater Res A*. 2007;80(1):206–215. doi:10.1002/jbm.a.30836
83. Weinhold M, Soubatch S, Temirov R, et al. Structure and bonding of the multifunctional amino acid l -DOPA on Au(110). *J Phys Chem B*. 2006;110(47):23756–23769. doi:10.1021/jp064956t
84. Lee BP, Messersmith PB, Israelachvili JN, et al. Mussel-inspired adhesives and coatings. *Annu Rev Mater Res*. 2011;41:99–132. doi:10.1146/annurev-matsci-062910-100429
85. Jo S, Kang SM, Park SA, et al. Enhanced adhesion of preosteoblasts inside 3 D PCL scaffolds by polydopamine coating and mineralization. *Macromol Biosci*. 2013;13(10):1389–1395. doi:10.1002/mabi.201300203
86. Palladino P, Bettazzi F, Scarano S. Polydopamine: surface coating, molecular imprinting, and electrochemistry-successful applications and future perspectives in (bio)analysis. *Anal Bioanal Chem*. 2019;411(19):4327–4338. doi:10.1007/s00216-019-01665-w
87. Zhang C, Gong L, Xiang L, et al. Deposition and adhesion of polydopamine on the surfaces of varying wettability. *ACS Appl Mater Interfaces*. 2017;9(36):30943–30950. doi:10.1021/acsami.7b09774

88. Kao CT, Lin -C-C, Chen Y-W, et al. Poly(dopamine) coating of 3D printed poly(lactic acid) scaffolds for bone tissue engineering. *Mater Sci Eng C Mater Biol Appl*. 2015;56:165–173. doi:10.1016/j.msec.2015.06.028
89. Cho HJ, Madhurakkat Perikamana SK, Lee J-H, et al. Effective immobilization of BMP-2 mediated by polydopamine coating on biodegradable nanofibers for enhanced in vivo bone formation. *ACS Appl Mater Interfaces*. 2014;6(14):11225–11235. doi:10.1021/am501391z
90. Lee SJ, Won J-E, Han C, et al. Development of a three-dimensionally printed scaffold grafted with bone forming peptide-1 for enhanced bone regeneration with in vitro and in vivo evaluations. *J Colloid Interface Sci*. 2019;539:468–480. doi:10.1016/j.jcis.2018.12.097
91. Li L, Lu H, Zhao Y, et al. Functionalized cell-free scaffolds for bone defect repair inspired by self-healing of bone fractures: a review and new perspectives. *Mater Sci Eng C Mater Biol Appl*. 2019;98:1241–1251. doi:10.1016/j.msec.2019.01.075
92. Sánchez-Duffhues G, Hiepen C, Knaus P, et al. Bone morphogenetic protein signaling in bone homeostasis. *Bone*. 2015;80:43–59. doi:10.1016/j.bone.2015.05.025
93. Suliman S, Xing Z, Wu X, et al. Release and bioactivity of bone morphogenetic protein-2 are affected by scaffold binding techniques in vitro and in vivo. *J Control Release*. 2015;197:148–157. doi:10.1016/j.jconrel.2014.11.003
94. Halloran D, Durbano HW, Nohe A. Bone morphogenetic protein-2 in development and bone homeostasis. *J Dev Biol*. 2020;8(3). doi:10.3390/jdb8030019
95. Liu X, Yin M, Li Y, et al. Genipin modified lyophilized platelet-rich fibrin scaffold for sustained release of growth factors to promote bone regeneration. *Front Physiol*. 2022;13:1007692. doi:10.3389/fphys.2022.1007692
96. Wang M, Wang C, Zhang Y, et al. Controlled release of dopamine coatings on titanium bidirectionally regulate osteoclastic and osteogenic response behaviors. *Mater Sci Eng C Mater Biol Appl*. 2021;129:112376. doi:10.1016/j.msec.2021.112376
97. Ko E, Yang K, Shin J, et al. Polydopamine-assisted osteoinductive peptide immobilization of polymer scaffolds for enhanced bone regeneration by human adipose-derived stem cells. *Biomacromolecules*. 2013;14(9):3202–3213. doi:10.1021/bm4008343
98. Croes M, Oner FC, Kruyt MC, et al. Proinflammatory mediators enhance the osteogenesis of human mesenchymal stem cells after lineage commitment. *PLoS One*. 2015;10(7):e0132781. doi:10.1371/journal.pone.0132781
99. Ge L, Cui Y, Cheng K, et al. Isopsoralen enhanced osteogenesis by targeting AhR/ERα. *Molecules*. 2018;23(10):2600. doi:10.3390/molecules23102600
100. Huang Q, Liu Y, Ouyang Z, et al. Comparing the regeneration potential between PLLA/Aragonite and PLLA/Vaterite pearl composite scaffolds in rabbit radius segmental bone defects. *Bioact Mater*. 2020;5(4):980–989. doi:10.1016/j.bioactmat.2020.06.018
101. Zhao L, Zhao J, Tuo Z, et al. Repair of long bone defects of large size using a tissue-engineered periosteum in a rabbit model. *J Mater Sci Mater Med*. 2021;32(9):105. doi:10.1007/s10856-021-06579-7
102. Wang JS, Mazur CM, Wein MN. Sclerostin and osteocalcin: candidate bone-produced hormones. *Front Endocrinol*. 2021;12:584147. doi:10.3389/fendo.2021.584147
103. Kim HJ, Kim WJ, Ryoo HM. Post-translational regulations of transcriptional activity of RUNX2. *Mol Cells*. 2020;43(2):160–167. doi:10.14348/molcells.2019.0247
104. Bai X, Wang D, Zhen L, et al. Design and micromanufacturing technologies of focused piezoelectric ultrasound transducers for biomedical applications. *Int J Extreme Manuf*. 2024;6(6):062001. doi:10.1088/2631-7990/ad62c6